Production of Geopolymers from Fly Ash for Wastewater Treatment

Ana Paula Silva Natal

Thesis report submitted to

Escola Superior de Tecnologia e Gestão

Instituto Politécnico de Bragança

Master Degree in

Chemical Engineering

Supervisors:

Prof. Dr. Helder Teixeira Gomes

Prof. Dr. Pricila Marin

Dr. José Luis Díaz De Tuesta

Bragança

2023

Production of Geopolymers from Fly Ash for Wastewater Treatment

Ana Paula Silva Natal

Thesis report submitted to **Escola Superior de Tecnologia e Gestão** of **Instituto Politécnico de Bragança** to obtain the Master Degree in Chemical Engineering in the ambit of the double diploma with the **Universidade Tecnológica Federal do Paraná - Câmpus Londrina**

Supervisors:

Prof. Dr. Helder Teixeira Gomes

Prof. Dr. Pricila Marin

Dr. José Luis Díaz De Tuesta

Bragança

2023

ACKNOWLEDGEMENTS

First, I would like to express my deepest gratitude to my parents, Luciana and Paulo, for always believing in me and for their support. I also want to thank my brother Daniel for all that we share and learn from each other.

To my best friend and life partner, João Marcelo, I am immensely grateful for the support, encouragement, partnership, and love that you have provided me throughout this and all the stages of my life.

I sincerely thank my supervisors, Professor Dr. Helder Teixeira Gomes, from the Polytechnic Institute of Bragança (IPB), for entrusting me with this research and for all the necessary support given in this process. I am also grateful to Dr. José Luis Díaz de Tuesta for his teachings and guidance during this work. I thank Professor Dr. Pricila Marin, from the Universidade Tecnológica Federal do Paraná (UTFPR), for her support and assistance despite the distance.

I would like to thank the entire research group for their teaching and immense help. I want to give special thanks to my friend Julia, who has been by my side since the beginning of this work, sharing every moment of this master's journey. I am also immensely grateful to Msc. Ana Paula for her essential help, patience, and dedication at all times during this past year. Her contributions were fundamental for the development of this work.

I want to extend my gratitude to all my friends that I met before and during my time at UTFPR-Londrina. I am grateful for the friends I made in Bragança, especially Matheus Bonifacio, who faced the challenges of the past year by my side, Rodrigo, for the shared moments, and Ramily, my roommate, who became a sister, giving support whenever I needed it and making lighter even the most difficult moments.

To UTFPR, for providing me the opportunity to study this double degree in Portugal, and to IPB, for offering the structure and professionals necessary to support the development of this work. I would also like to thank Sogama for providing the raw material for this research.

The authors are grateful to the Foundation for Science and Technology (FCT, Portugal) for financial support through national funds FCT/MCTES (PIDDAC) to CIMO (UIDB/00690/2020 and UIDP/00690/2020) and SusTEC (LA/P/0007/2020).

This work was financially suported by project “VALUECOMP - Valorización de compost procedente de residuos municipales mediante la obtención eficiente de productos de valor añadido” (0765_VALUECOMP_2_P), through FEDER under Program INTERREG.

ABSTRACT

Rapid waste generation presents environmental, economic, and social challenges. The circular economy concept aims to reintegrate waste into production cycles, including municipal solid waste (MSW). Geopolymers (GPs) derived from MSW ash offer valuable applications, especially as cost-effective and environmentally friendly adsorbents. This study focuses on developing geopolymeric adsorbents using MSW fly ash (FA) as a precursor and evaluating their efficacy in treating wastewater containing gallic acid (GA). Specific objectives include characterizing the FA, optimizing geopolymer production through a Design of Experiment, and assessing the performance of the produced GPs as adsorbents. The experimental design in this study employed a Box-Behnken design (BBD) with three key factors: Si/Al mass ratio, NaOH molar concentration, and Na_2SiO_3/NaOH mass ratio. Material characterization was conducted using ICP-OES, porosimetry and surface area analysis, FT-IR, SEM, XRD, acid-base character, and pHpzc determination. Adsorption tests included studying the kinetics using pseudo-first-order and pseudo-second-order models and intraparticle diffusion. Equilibrium isotherms were analyzed using the Freundlich and Langmuir models. Statistical analysis indicated the Si/Al ratio as the most significant factor for GA removal. Characterization of the GPs and FA revealed FA's composition as a suitable source for aluminosilicate synthesis. Porosimetry and surface area analysis demonstrated substantial improvements in the GPs compared to FA, with GP-13 exhibiting the largest surface area equal to 61 m^2/g. FT-IR analysis confirmed geopolymerization, while SEM analysis revealed structural variations between the GPs and unreacted FA particles in the GPs. XRD analysis confirmed the amorphous nature of the produced materials and the predominance of calcite. Acid-base characterization demonstrated the basic nature of the GPs, with pHpzc values around 8, showing that electrostatic attraction between the positively charged GPs and GA contributed significantly to the adsorption process. Adsorption kinetics revealed a favorable fit to the pseudo-first-order model, with rapid initial adsorption reaching equilibrium at approximately 200 minutes. Equilibrium studies favored the Freundlich model, indicating favorable adsorption conditions with a significant affinity between GA and the GPs. GP-6 exhibited the highest maximum adsorption capacity of 75.839 mg/g. In conclusion, all the produced GPs showed efficiency to adsorb GA.

Keywords: Geopolymers; Municipal Solid Waste; Fly Ash; Adsorption; Circular Economy.

RESUMO

A geração rápida de resíduos apresenta desafios ambientais, econômicos e sociais. O conceito de economia circular visa reintegrar os resíduos nos ciclos de produção, incluindo os resíduos sólidos urbanos (RSU). Geopolímeros (GPs) derivados de cinzas de RSU oferecem aplicações valiosas, especialmente como adsorventes econômicos e ecologicamente corretos. Este estudo foca no desenvolvimento de adsorventes geopoliméricos utilizando cinzas volantes de RSU como precursor e avaliando sua eficácia no tratamento de águas residuais contendo ácido gálico (AG). Os objetivos específicos incluem caracterizar as cinzas volantes, otimizar a produção de geopolímeros por meio de um Design Experimental e avaliar o desempenho dos GPs produzidos como adsorventes. O delineamento experimental utilizado foi um Design de Box-Behnken (BBD) com três fatores principais: razão mássica Si/Al, concentração molar de NaOH e razão mássica Na_2SiO_3/NaOH. A caracterização dos materiais foi realizada utilizando ICP-OES, porosimetria e análise de área superficial, FT-IR, SEM, XRD, caracterização ácido-base e determinação do pHpzc. Os testes de adsorção incluíram o estudo da cinética utilizando modelos de pseudo-primeira ordem e pseudo-segunda ordem, além da difusão intrapartícula. As isotermas de equilíbrio foram analisadas utilizando os modelos de Freundlich e Langmuir. A análise estatística indicou a razão Si/Al como o fator mais significativo para a remoção de AG. A caracterização dos GPs e das cinzas volantes revelou a composição das cinzas volantes como uma fonte adequada para a síntese de aluminossilicatos. A análise de porosimetria e área superficial demonstrou melhorias significativas nos GPs em comparação com as cinzas volantes, com o GP-13 apresentando a maior área superficial igual a 61 m^2/g. A análise de FT-IR confirmou a geopolimerização, enquanto a análise de SEM revelou variações estruturais entre os GPs e partículas de cinzas volantes não reagidas nos GPs. A análise de XRD confirmou a natureza amorfa dos materiais produzidos e a predominância de calcita. A caracterização ácido-base demonstrou a natureza básica dos GPs, com valores de pHpzc em torno de 8, mostrando que a atração eletrostática entre os GPs carregados positivamente e o AG contribuiu significativamente para o processo de adsorção. A cinética de adsorção revelou um ajuste favorável ao modelo de pseudo-primeira ordem, com rápida adsorção inicial alcançando o equilíbrio em aproximadamente 200 minutos. Os estudos de equilíbrio favoreceram o modelo de Freundlich, indicando condições favoráveis de adsorção com afinidade significativa entre o

AG e os GPs. O GP-6 apresentou a maior capacidade máxima de adsorção de 75.839 mg/g. Em conclusão, todos os GPs produzidos mostraram eficiência na adsorção de AG.

Palavras-chave: Geopolímeros; Resíduos Sólidos Urbanos; Cinzas Volantes; Adsorção; Economia Circular.

TABLE OF CONTENTS

LIST OF FIGURES

LIST OF TABLES

LIST OF ACRONYMS

AC	Activated Carbon
BBD	Box-Behnken design
CCD	Central Composite Design
FA	Fly ash
FT-IR	Fourier transform infrared spectroscopy
GA	Gallic acid
GNI	Gross National Income
GPs	Geopolymers
HPLC	High-performance liquid chromatography
ICP	Inductively Coupled Plasma
ICP-OES	Inductively Coupled Plasma Optical Emission Spectroscopy
MSW	Municipal Solid Waste
PZC	Point of zero charge
RSM	Response surface method
SEM/EDS	Scanning electron microscopy/ Energy dispersive spectroscopy
XRD	X-ray diffraction

1 INTRODUCTION

Population growth, rapid urbanization, and increasing consumption are some factors that have contributed to the growing production of solid waste over the years[1]. Overall, the world generates 2.10 billion tons of municipal solid waste (MSW) per year, and by 2050 this number is expected to reach 3.40 billion tons[2]. Thus, solid waste represents a sign of inefficiency and misallocated resources for the current society, becoming one of today's major environmental problems[3].

Given this, the European Commission adopted the new circular economy (CE) action plan in March 2020. This plan aims at sustainable consumption with the lowest possible loss of resources, where those resources stay as long as possible within the production process, mitigating the problem involving the large volume of solid waste in landfills and sparing nature from using new resources[4]. For such goals to be achieved, action strategies are needed and that are defined in the European Commission's Action Plan document. The first is to ensure that the product has been sustainable since its initial design; being necessary that the product presents some characteristics such as greater durability, the possibility of reuse, increased content of recycled materials, stimulated remanufacturing, and reduced carbon footprints, among others[5]. It is also relevant to provide circularity in production processes, to allow reductions in energy and raw material costs, and consequently in monetary value[5].

The alternative of using MSW in the generation of products instead of new raw materials can mitigate the problems involving the large volume of MSW in landfills and save the environment from exploiting new resources, fitting the CE proposal[6]. This MSW can be reinserted into the economy as an energy source through conventional and hydrothermal incineration, pyrolysis, and thermochemical and hydrothermal liquefaction[7]. Furthermore, it is also possible to use MSW to produce inorganic materials such as geopolymers (GPs)[8].

GPs are ceramic materials usually made at low temperatures through a geopolymerization reaction. They can be produced from nuclear waste, rice husk ash, natural fiber, waste glass, plastic, municipal solid incineration ash, and many others[8]. Numerous studies have used incinerated MSW ash, either MSW bottom ash or fly ash (FA), as a source of aluminosilicate[9].

Their composition influences the application of these materials since different precursors result in different structures and characteristics of the material. Thus, GPs can be

used in diverse fields such as aeronautical engineering[10], nuclear industry[11], archaeological research[12], construction materials[9] and as adsorbent materials for water treatment[13].

Some characteristics of GPs contribute to their use as adsorbent materials, such as rapid strength, low cost, environmental friendliness, good ion exchange capacity, and adequate solidification of toxic waste. These materials are promising when used for water treatment, proving efficient for dye removal in aqueous solutions[14], metal removal in wastewater[15], and anionic surfactant removal in aqueous solutions[16].

2 STATE OF THE ART

2.1 GENERATION OF SOLID WASTE

According to the Waste Framework Directive[17], waste is "any substance or object which the holder disposes of or is required to dispose of." Numerous types of waste depend on their characteristics and origin; some examples are MSW, agricultural and animal waste, industrial waste, medical waste, radioactive waste, construction and demolition debris, and oil and gas production waste. These come from many different human activities[18]. Figure 1 shows the primary sources of solid waste generation in the European Union (EU) in 2020[19].

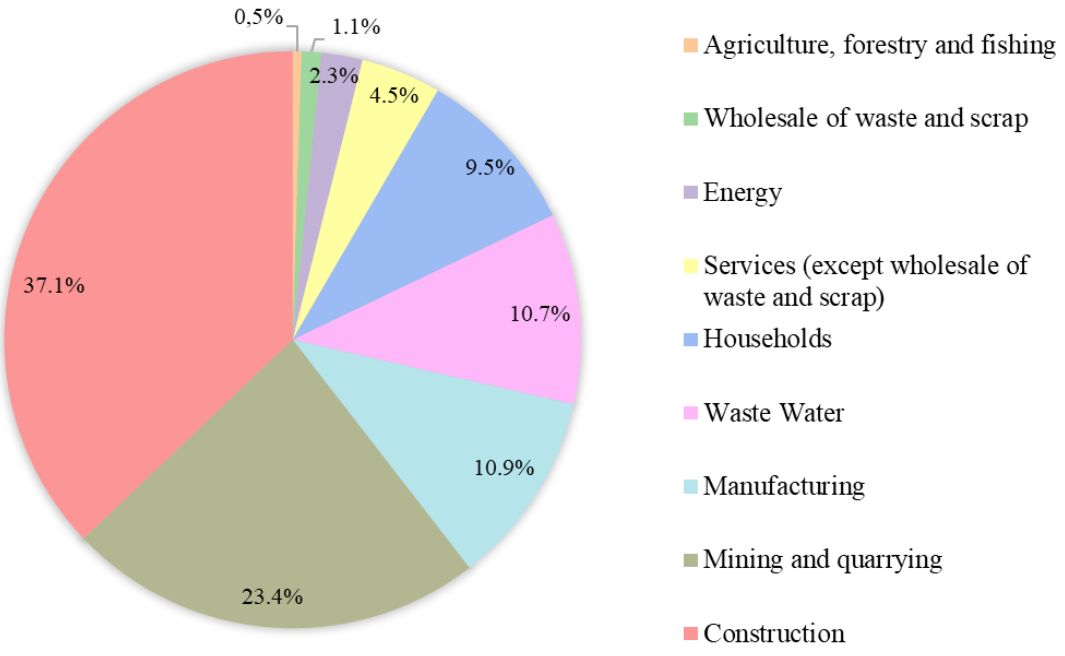

Figure 1: Distribution of the primary sources of waste in the EU (adapted from [19]).

Over the years, the worldwide increase in solid waste production caused several environmental problems such as air pollution[20], soil[21], and water[22] contamination, climate change[23], and directly affecting several ecosystems and species[24].

Rapid industrialization, urbanization, increase in consumption and production, and especially population growth, contribute to solid waste generation[25]. Table 1 shows the growth of municipal waste and population in the EU from 2014 to 2019[26].

Table 1: Growth of municipal waste and population in the EU from 2014 to 2019 (adapted from [26,27]).

Year	Municipal Waste (10^3 m^3)	Population (10^6)
2014	211.9	506.9
2015	213.4	508.2
2016	218.0	510.1
2017	221.0	511.8
2018	221.6	512.4
2019	224.0	513.5

From Table 1, it is possible to observe the direct relation between population growth and municipal waste production. In 2019 the population grew by 1.30% compared to 2014, while the amount of municipal waste increased by 5.71% compared to the same year.

2.1.1 MUNICIPAL SOLID WASTE

MSW is a non-homogeneous mixture of solid waste generated in households, offices, restaurants, schools, stores, and other institutions. It comes from the most varied commercial, institutional, and recreational occasions. For this reason, they present a highly varied composition depending on where it was generated. They may contain paper, plastic, glass, food waste, medicine, and even small amounts of hazardous waste, such as light bulbs, batteries, and chemicals[28]. Figure 2 shows the variation in the composition of MSW comparing countries with different income levels[29].

Income level is a classification given to countries according to gross national income (GNI) per capita. GNI is the total income the country receives from its residents and businesses, which is divided by the total population. Depending on this value, the country is classified as low income (<$1,046.00), lower-middle-income ($1,046.00 – $4,095.00), upper-middle income ($4,096.00 – $12,695.00) and high income (> $12,695.00)[30].

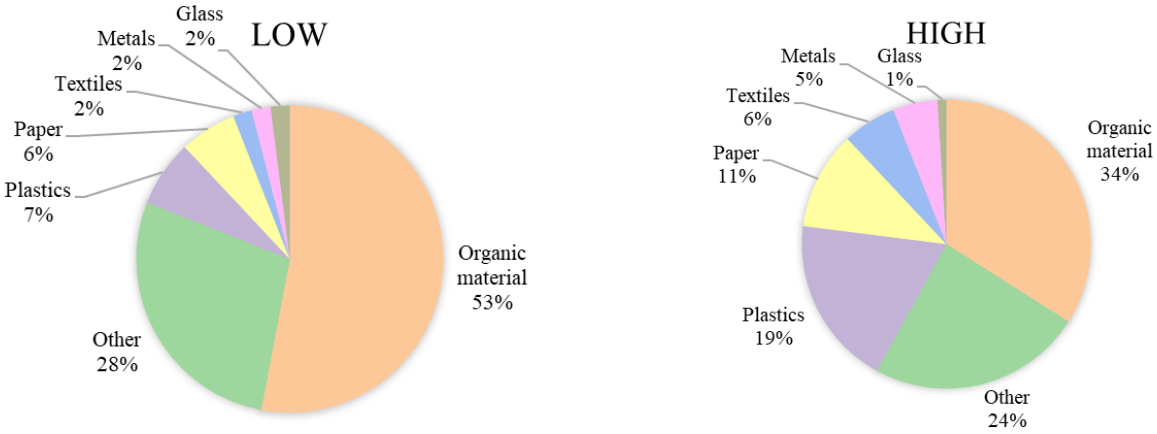

Figure 2: MSW composition in countries with different income levels (adapted from [29])

Despite its variable composition in the two compared scenarios, most of the composition of both places is organic matter; hence, it is generally accepted that MSW is primarily composed of organic matter, mainly from food scraps[31]. The variation of its composition influences its chemical and physical characteristics, such as density, amount of moisture, and calorific value, which affect the choice of the ideal type of treatment for such waste[29].

The amount of MSW generated is significant, and in the EU, each citizen produces, on average, half a ton of this type of waste per year. In counterpoint to the large amount produced, MSW by itself has little economic value and, if not treated properly, has great potential to cause adverse effects on the environment and human health[32], to increase greenhouse gas emissions[33], intensify water pollution[34] and soil[35], as well as corroborating the spread of diseases[36].

Some predominant solid waste treatment techniques in the EU are recycling, landfilling, incineration, and composting. In 2000, the most common treatment used was landfill (51.1%) however, other types of treatment have been gaining space because they are more advantageous and environmentally friendly, as is the case of recycling[29]. The distribution of the main types of waste treatment in 2000, 2010, and 2020 in the EU is shown in Figure 3[37].

European legislation implemented over the years is mainly responsible for these changes. For example, Directive 62/1994 on packaging and packaging waste 2001 set that member states had to recover at least 50% of all packaging placed on the market, with a revised target of 65% of packaging waste being recycled by 2025. Another example is Directive 31/1999 on landfill. It stipulated that member states were obliged to reduce the amount of biodegradable municipal waste going to landfills to 75% in 2006, 35% in 2016, and 10% in 2035. Thus, countries were

directed to adopt different ways of managing MSW, such as composting and incineration, to avoid landfilling the organic fraction of municipal waste[37].

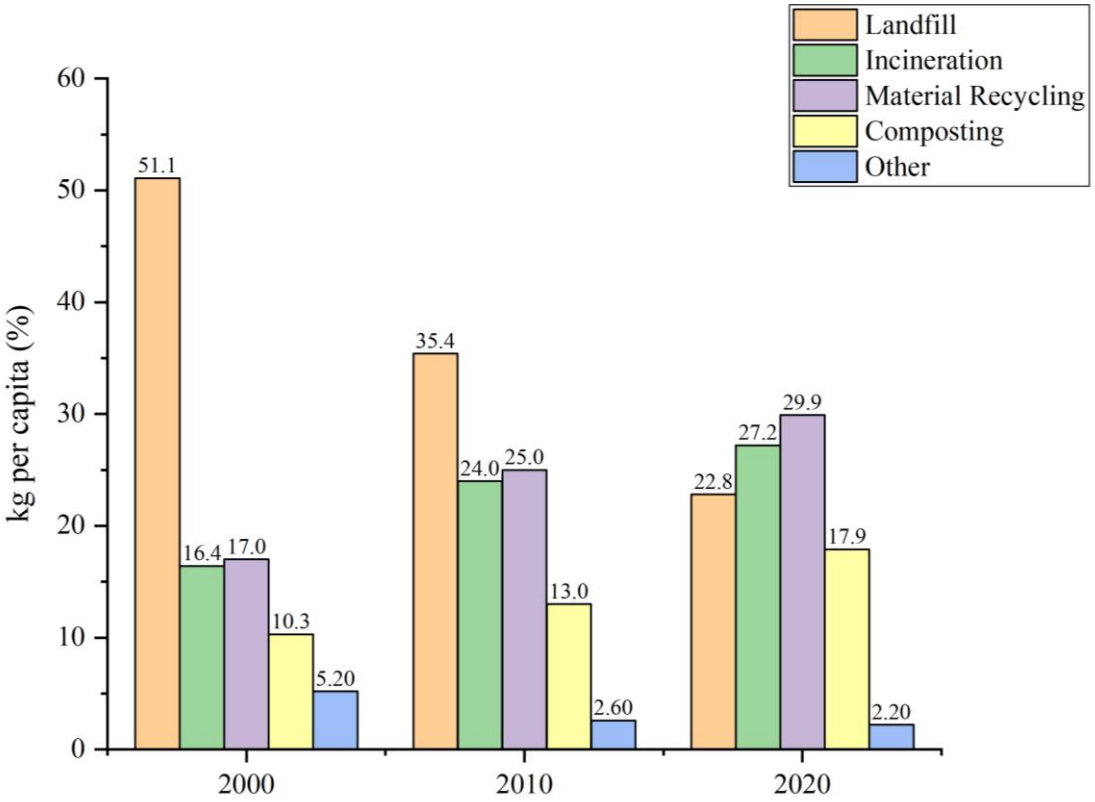

Figure 3: MSW treatment in the EU in 2000, 2010, and 2020 (adapted from [37]).

Despite changing legislation, landfills are still the most used treatment in the world, especially in low-income countries, due to their low cost compared to the other processes. This type of treatment can be defined as places to dispose of solid waste buried in the ground to compact and reduce its volume[38]. Regardless of the facilities presented by sanitary landfills, these can represent a significant environmental risk. First, the waste discarded there inevitably releases hazardous constituents into the environment[39]. In addition, leachate is produced, a contaminant liquid generated in landfills mainly because of the percolation of the rainwaters in these MSW disposal sites. This fluid has excellent potential for soil and surface and groundwater pollution[40].

Another technique for MSW treatment is incineration. This thermal treatment consists of burning the waste material and usually has an energy and heat recovery system[33]. Initially, this treatment was only used for waste volume reduction since it can reduce 90% of the initial waste volume[41] and it had a high potential for air pollution[42]. Recent incineration plants are suitable

for advanced air pollution control techniques and have an energy recovery system[41]. Recent studies show that the bottom and fly ashes produced during incineration can be used to produce construction materials[43].

It is important to emphasize that MSW recycling is an excellent strategy to reduce the negative environmental impacts and to promote sustainable development by saving the use of new resources, reducing the amount of waste sent to landfills, and other positive consequences[46]. Due to recycling being based on recovering solid waste and reprocessing them into products, materials, or substances for another purpose or of the same origin[44], this procedure is one technique that most favors the environment and is directly aligned with the CE. MSW has materials that can be recycled, like glass, paper, plastics, and metals[45]. Unfortunately, only 38% of MSW is recycled, but the European Commission's target for 2030 is to increase this value to 65%[44]. For this, among other aspects, it is necessary to review laws and policies related to solid waste and to make society aware of the importance of starting the separation of waste at home[45].

Composting is a biological process involving the aerobic degradation of organic matter conducted under controlled moisture, self-heating, and temperature below 50 °C[46]. The mature compost can eliminate phytotoxicity, weed seeds, and pathogens and can avoid microbial competition with plant roots for nitrogen and oxygen by stabilizing the material concerning these elements[47]. Therefore, it is possible to obtain a stable organic matter that can be used as a fertilizer[51] through composting.

2.2 CIRCULAR ECONOMY

Given the increasing solid waste production worldwide and the environmental impacts it causes, there is increasing attention from authorities regarding environmental issues and sustainable growth. The most recent action plan adopted by the EU, announced in March 2020, promotes actions encouraging CE to save the use of new natural resources by reinserting waste in the production cycle, giving it a new economic value[5].

According to Suarez-Eiroa[48], CE can be defined as:

> The Circular Economy is a regenerative production-consumption system that aims to maintain extraction rates of resources and generation rates of wastes and emissions under suitable values for planetary boundaries, by closing the system, reducing its size, and maintaining the resource's value as long as possible within the system,

> mainly leaning on design and education, and with a capacity to be implemented at any scale[48].

The ecological economist Kenneth E. Boulding introduced the concept of CE into the academic literature when, in 1966, he criticized the "linear cowboy economy" of the past and described a future as a "spaceship economy" in which all resources used were returned to the system. The holistic approach of creating circular loops of material, energy, and waste flows covering all activities in society is the main characteristic of the CE that distinguishes it from other approaches to reducing the consumption of natural resources[49].

There are three levels on which initiatives for implementing such economy practices can be divided: the micro, meso, and macro. The micro level relates to the initiatives often appearing in the literature as the 4R Principle: Reduce, Reuse, Recycle and Recover. The first term, reduction, is related to minimizing the use of raw materials, energy, and waste generation. Using a resource several times to save the use of new ones is the principle of reuse. And the reprocessing of waste materials to generate new products is the concept of recycling[49]. Initiatives related to collaboration between chains and sectors, where the waste from one company becomes the raw material for another, are related to the meso level. At the macro level are the efforts made by governments and policy makers, such as the action plan adopted by the European Commission[49].

CE is becoming increasingly relevant and is of paramount importance for sustainable development, bringing countless environmental benefits, such as the reduction of greenhouse gases, with an expected decline of 48% in the year 2030 and 83% in the year 2050, compared to the figures for the year 2012, besides social benefits with the creation of new jobs with the idea of substituting products for services and also improving the monitoring and dissemination of practices that collaborate with recycling and reuse of waste. The prospect is to create 178,000 new jobs by 2030. And, finally, economic benefits, since the application of the CE can bring cost savings to several industries, with estimated savings in the cost of raw materials about USD 340-630 billion per year only in the EU[44].

For the evolution of the linear economy to a circular economy, some actions and targets are required to "close the loop" of the life cycle of products, giving them a new economic value instead of simply discarding them. EU sets many such targets, and they aim at common goals such as recycling 65% of MSW and 75% of packaging waste by 2030, reducing landfills to a

maximum of 10% of MSW by 2030, and banning landfills for separately collected waste, and promoting economic instruments to discourage landfills, among other objectives[44].

MSW can be reinserted into the economic cycle, promoting CE in several ways: production of biodegradable plastics from food waste[50], synthesis of biogas from agricultural waste[51], valorization of medical waste through pyrolysis to produce bio-oil[52], and production of GPs with the potential to be used as road construction materials from residual ash and slag from thermal power plants[53].

2.2.1 VALORIZATION OF SOLID WASTE

Solid waste valorization is related to any treatment which has the purpose of reusing, recycling, or composting from wastes resulting in usable products with added value or a renewable energy source[54]. These practices have great relevance mainly because they reduce the volume of waste in landfills and decrease the emission of greenhouse gases and other environmental impacts[55].

MSW is a worthy, renewable, economic waste that can be retrieved as solid, liquid or gaseous fuels. There are various techniques for transforming waste into energy, such as composting, incineration, gasification, pyrolysis and production of biofuels. Among these techniques main advantages is the reduction of the dependence on fossil fuels as the primary energy source for domestic and commercial applications[60]. The potential of MSW for renewable energy generation has been studied in recent years to evaluate its viability and efficiency for commercial-scale application.

Furthermore, the organic fraction of MSW has enormous potential for producing fuel and value-added products since it contains widely available biodegradable materials[56]. The development of biogas plants for energy production has been increasingly encouraged, given the energy and climate policies in the EU and the introduction of numerous support schemes to promote renewable resources. Biogas can generate energy such as electricity, heat, and fuel through anaerobic digestion, adding economic, environmental, and climate benefits. Moreover, it can also be upgraded to biomethane and injected into the natural gas system or used in transport vehicles, with appropriate purification to remove trace gases such as H_2S, water, and CO_2[57].

Another way to valorize waste is through recycling; this technique reduces the consumption of primary resources through secondary materials made from recycled waste. EU waste management targets are focused on raising recycling rates. Recycling rates for MSW have been slowly increasing in Europe; less than half of all solid waste generated on the continent is recycled, indicating some progress toward using more waste as a resource and achieving a circular economy[58].

The Directive 2008/98/EC aims to move the EU closer to a "recycling society" by reducing waste generation and valorizing waste. In particular, by requiring measures to ensure source separation, collection, and recycling of priority MSW streams. Before undergoing recovery operations that provide for the most environmentally favorable destination, waste shall be collected separately, if technically, environmentally, and economically practicable, to facilitate or improve its recovery potential. If necessary, member states should encourage the separation of hazardous compounds from waste streams to achieve environmentally sound management[17].

Some of the other objectives of the EU to encourage recycling are: to introduce landfill restrictions on all waste suitable for recycling or energy recovery from 2030; the preparation for reuse and recycling of MSW should raise to a minimum of 55%, 60%, and 65% by weight by 2025, 2030 and 2035, respectively; the use of recycled materials should be supported by member states, following the waste hierarchy and, whenever possible, they should not support the landfilling or incineration of recyclable materials[59].

2.2.1.1 FLY ASH

Fly ash is the finest of coal ash particles, usually light bronze, the size of silt and clay. Their properties and components may vary with coal composition and plant operating conditions. But in general, the components of FA are SiO_2, Al_2O_3, CaO, and Fe_2O_3, which exist in the form of amorphous and crystalline oxides or various minerals[60].

This particulate material is produced from coal combustion in thermal power plants, the non-combustible material being coal, and a small amount of carbon remains from incomplete combustion[61]. Particle filtration equipment usually captures it from the flue gases before the combustion gases reach the chimneys or mainly electrostatic precipitator systems[62].

As a result of its large production, there is a growing need to reduce its accumulation, improve the way it is disposed of, and focus mainly on how to reuse this material, enabling it to be put back into the economy[63]. FA is a versatile material that can be used in many areas and can be applied as a soil amendment[64] and as fertilizer on agricultural land[65], because of properties like its chemical composition and its physical properties such as surface area, porosity, and particle size distribution it can also be used as an adsorbent[66] and is recently being used for the production of GPs[60].

2.3 GEOPOLYMERS

By the end of the 1970s, Professor Joseph Davidovits guided his studies in fireproof polymers, and the term "geopolymer" was introduced. This discovery of geosynthesis that produces inorganic polymeric materials has attracted much interest in the academic and commercial spheres over the last few years and is used for several industrial applications[67].

GPs are aluminosilicate inorganic polymers that result from the polycondensation of inorganic compounds, aluminosilicates, or aluminosilicate wastes, with alkalis or acids cured at ambient temperature[68]. GPs have an amorphous three-dimensional structure with a random 3-D array of tetrahedrally-coordinated AlO_4 and SiO_4 units in a random arrangement, charge-stabilized by the hydrated alkali metal cations[69], as shown in Figure 4[70].

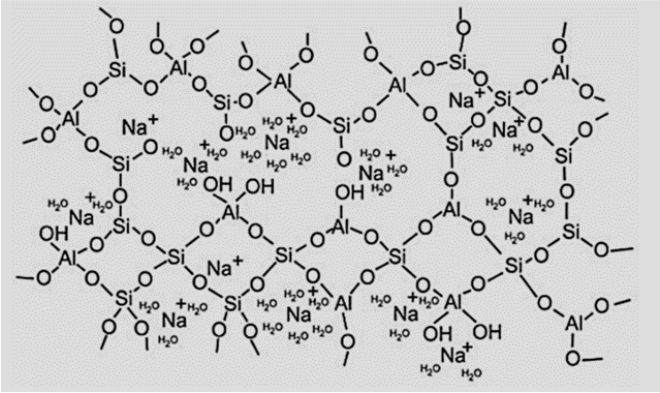

Figure 4: Geopolymer Structure[70]

A geopolymerization reaction produces these eco-friendly materials. This process mainly involves dissolution, gelation, and condensation reactions occurring parallel to form the material of interest. The geopolymer formation depends on the alkali activation of aluminosilicate materials such as metakaolin, FA, and granulated blast furnace slag. Beyond

these more traditional aluminosilicate materials, new ones that have the potential to be used as precursors are constantly being discovered, such as biomass FA, bottom ash, waste glass, and sedimentary rock powder. Sodium and potassium hydroxide with sodium and potassium silicate are the most common alkali activators synthesizing geopolymer[71].

The steps to produce GPs are generally simple, as shown in Figure 5[71]. About the geopolymerization reaction, the first step of the reaction consists of the action of the strong alkali solution, which leads to the formation of free AlO_4 and SiO_4 tetrahedral units through the break of Si-O and Al-O bonds, obtaining the monomers. So, these two groups have an alternate conjunction to produce polymorphic precursors with the release of water molecules[62].

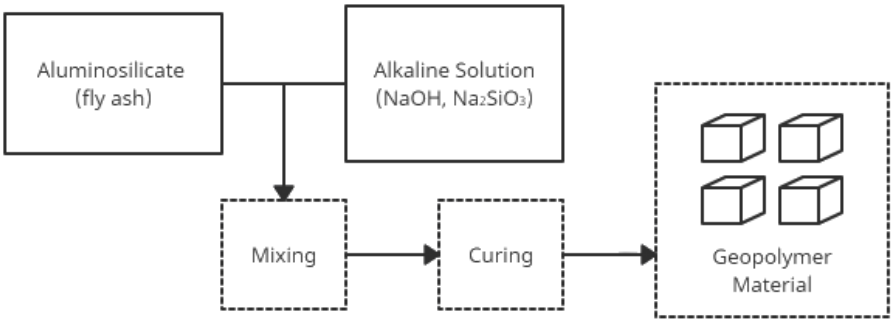

Figure 5: Geopolymer Production Steps (adapted from [71]).

Alkali metal cations are in the framework to balance the negative charge of the aluminate ion. The monomer's interaction forms the geopolymer material from oligomers and synthesizes the 3D structure, as shown in Figure 6[76]. A vigorous mixing at this stage is necessary to ensure complete diffusion of the alkali species[72].

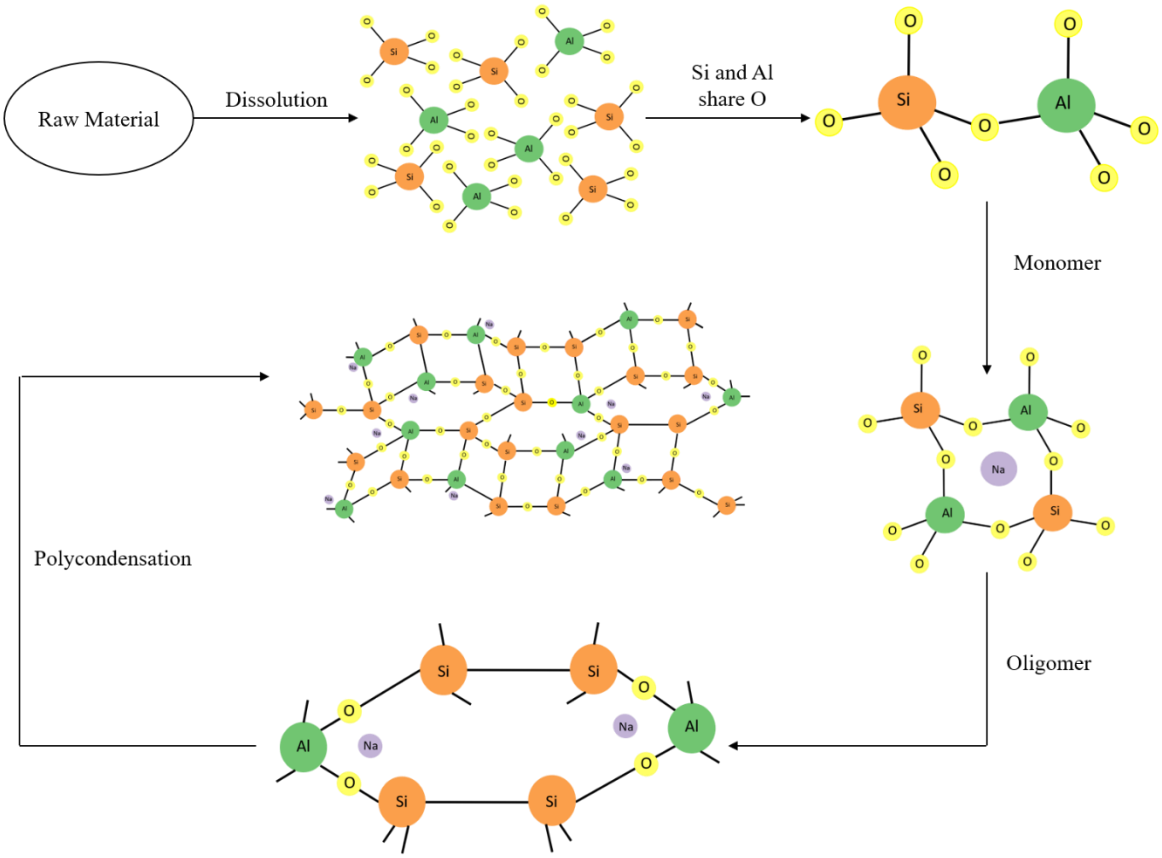

Figure 6: Geopolymerization (adapted from [73]).

The empirical formula of the formed geopolymer is $M_n [- (SiO_2)z - AlO_2]_n \cdot wH_2O$, where *M* represents the alkali cation such as potassium, sodium, or calcium, *n* the degree of polymerization, and *z* the molar ratio of silicon to aluminum[74]. The produced material must be exposed to temperatures below 100 °C to undergo the curing process. The resultant geopolymer has a solid and stable structure and pores, an advantageous feature for the adsorption process[71,74].

The composition of GPs influences their characteristics and applications. The Si/Al ratio affects the hardness of the material, with a Si/Al ratio less than 3 resulting in a rigid geopolymer suitable for use as a construction material such as concrete or cement[75]. Furthermore, the higher this ratio, the larger the pore volume observed in the GPs[76]. The Na/Al ratio influences the polymerization process, interfering in the Si^{4+} and Al^{3+} dissolution step[75].

GPs are attractive mainly because they are environmentally friendly since they can be produced using precursors that would otherwise be discarded as waste glass[77], biomass FA[78], a red mug and rice husk[79] and sugarcane bagasse ash[80], among many others. The final

characteristics of the geopolymer depend on the used precursor and mix proportions and curing conditions[81].

GPs have a low CO_2 embodied material, so they were first developed to replace Portland cement[82]. Meanwhile, due to its advantages and attractive characteristics, there are more and more studies and development of new applications for GPs, for example, coating material, masonry units[83], catalysts[84], and also as an adsorbent for wastewater treatment for the removal of dyes[78] and heavy metals[85]. Table 2 shows some examples of GPs, their compositions, curing conditions, characteristics, and applications.

Table 2: Geopolymer Examples.

Ref.	Precursor	Si/Al	SiO_2/Na_2O	Alkaline activator	Curing conditions	Main properties	Application
[86]	Clay and sand	-	-	NaOH (10 M)	24 h at room temperature and 24 h at 120 °C	Compressive strength of 14.92 MPa	Concrete
[87]	Low illitic raw clay and waste brick	5.06	-	KOH (10M)	24 h at room temperature	Flexural strength of 13.7 MPa and water absorption	Bricks and tiles
[79]	Biomass fly ash	-	3.15	NaOH (10 M)	24 h at 40 °C	Extremely light and porous	Methylene blu removal
[88]	Fly ash and slag	-	-	NaOH (12 M)	120 h at room temperature	Axial compressive stress of 50-130 MPa	Structural concrete
[89]	Fly ash and silica fume	-	1.50	NaOH (10 M)	5 min at microwave radiation/24 h at room temperature	Compressive strength of 90 MPa (28 d)	Building material
[13]	MSW bottom ash and fly ash	-	-	NaOH (5 M)	72 h at 65 °C	High adsorption efficiency	Cationic dye removal
[90]	MSW incinerator fly ash and volcanic ash	2.74	0.66	NaOH (6 M)	24 h at room temperature	Moderated mechanical properties	Non-structural materials (bricks and paving stones)

2.4 WASTEWATER TREATMENT

Wastewater is generated from human activities, at home, in industry, hospitals, and agricultural sector. It has a complex composition with significant solids, dissolved and particulate matter, microorganisms, nutrients, heavy metals, and micro-pollutants[91]. This type of waste is directly related to serious environmental problems such as the water crisis and environmental deterioration and can be one of the factors causing water pollution[92].

Factors such as spills or leaks from oil and chemical containers[93], rapid urbanization, industrialization, the formation of city clusters[94], and the excessive use of chemical fertilizers and pesticides[95], untreated and improperly disposed of as wastewater, are also factors that can cause water pollution. This problem has become a challenge all over the globe. It has been estimated that one-third of the world population can be affected by the lack of safe drinking water[113]. Thus, there is a growing demand and concern for the correct treatment of wastewater[100].

Wastewater treatment can be carried out through chemical, biological, and physical treatments or a combination of them. It can be defined as how water used or contaminated is restored to a desirable quality. Water can be treated to any desired quality level depending on its purpose, for example, for aquatic life, drinking water, or irrigation, although, as its purity increases, so does the cost of achieving that purity[96].

The selection of the treatment method to remove solids, including colloids, organic matter, nutrients, and soluble contaminants from the effluent depends on the characteristics and source of the water to be treated. Each treatment has its characteristics and is best suited for each type of situation in terms of cost, viability, efficiency, workability, reliability, environmental impact, sludge production, operational complexity, pre-treatment demands, and potentially toxic by-products. Several techniques can be used for wastewater treatment. These can be classified into conventional methods, established recovery processes, and emerging removal methods and their variations, as shown in Table 3.

Table 3: Technologies available for pollutant removal in aqueous matrices (adapted from [97]).

Conventional methods	Established recovery process	Emerging removal methods
Coagulation/flocculation	Solvent extraction	Advanced oxidation
Precipitation	Evaporation	Adsorption onto non-conventional solids
Biodegradation	Oxidation	Biosorption
Filtration (sand)	Electrochemical Treatment	Biomass
Adsorption using AC	Membrane Separation	Nanofiltration
	Membrane Bioreactors	
	Ion-Exchange	
	Incineration	

2.4.1 GALLIC ACID

Phenolic compounds are commonly found in wastewater from various industrial processes, including pharmaceutical, food, textile, fine chemical, and petrochemical industries. These compounds are known for their high toxicity and low biodegradability, making them a significant environmental concern. Therefore, extensive research has been conducted to find effective methods for their removal. Several treatment approaches have been explored, including chemical oxidation, membrane retention, and adsorption[98].

Gallic acid (GA), also known as 3,4,5-trihydroxybenzoic acid, is widely used as a standard solution to determine a sample's total amount of phenolic compounds. This is due to its stability and relatively low cost compared to other phenolic compounds. Gallic acid belongs to the class of hydroxybenzoic acid derivatives and is classified as a simple phenolic acid. Its selection as a standard is based on its availability as a stable and pure substance, making it suitable for accurate quantification of phenolic compounds in various samples[99].

Gallic acid is a phenolic compound that occurs naturally in various plant sources, including grape seeds and green and black tea. Its chemical structure (Figure 7), which includes a carboxylic acid and three hydroxyl groups, contributes to its potential antioxidant capacity.

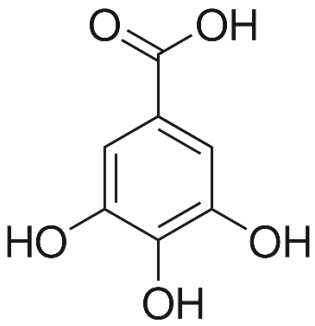

Figure 7: Structure of GA.

GA has attracted significant attention from the pharmaceutical and chemical industries due to its diverse properties and commercial applications. This compound has demonstrated various beneficial characteristics, including antifungal, antimicrobial, and anticancer activities. Additionally, GA has been recognized for its significant anti-inflammatory potential and antioxidant properties [100].

The wide range of properties exhibited by GA has led to numerous studies exploring its various applications. In the pharmaceutical field, research has focused on investigating its pharmacological activity and understanding the underlying molecular mechanisms[101]. In the food industry, recent studies have explored the use of GA in the development of antioxidant films for food packaging, aiming to enhance the shelf life and quality of food products[102]. Additionally, GA has been studied for its potential application in cosmetics, with research investigating its efficacy and suitability for use in cosmetic formulations[103]. These diverse areas of study highlight the versatility of GA and its potential for application in different industries.

2.4.2 ADSORPTION

Adsorption is an efficient approach for removing numerous undesirable substances from wastewater and has many advantages, such as ease of use, flexibility, low energy consumption, eco-friendliness, simple and versatile design, and cost-effectiveness.

Adsorption is indeed a commonly employed process in tertiary wastewater treatment. Tertiary treatment serves as the final stage of wastewater treatment, following primary and secondary treatment processes. While primary treatment removes solid materials and secondary treatment focuses on biological processes to reduce organic matter and pathogens, tertiary treatment aims to achieve further purification of the wastewater[104].

Tertiary treatment, also known as advanced wastewater treatment, includes a series of supplementary processes designed to target residual contaminants that may persist after secondary treatment. These additional steps consist of coagulation, filtration, activated carbon adsorption for organic removal, reverse osmosis, and other disinfection steps[104].

Adsorption used in tertiary wastewater treatment effectively removes residual soluble organic matter and other chemical compounds that remain after the primary and secondary treatment stages. Some of the commonly used adsorbents are zeolites, oxides, polymeric adsorbents, and activated carbon[105]. There are many examples in the literature of adsorbent materials, such as activated carbons, biomaterials[106], clay materials, and even nanostructures such as fullerenes, carbon nanotubes, and graphene[107-109].

Factors including the properties of the fluids and pollutants to be adsorbed, the type of adsorbent, operating conditions, process configuration, regeneration, and waste disposal generally influence the economic and technical feasibility of adsorption processes[110].

Adsorption is a mass transfer process in which a molecule (adsorbate) from a fluid is shifted into a porous solid material, forming a superficial monomolecular layer on this material (adsorbent)[111]. This phenomenon occurs due to the difference in concentration and physical forces (physisorption) or by chemical bonds (chemisorption), and the reverse process is called desorption[112]. There are three mechanisms on which the adsorption process is based: steric, equilibrium, and kinetic[113].

In the first one, the steric separation mechanism, the pores of the solid must have a particular selective dimension that allows the molecules of interest to enter and excludes others. The equilibrium mechanism is based on the different abilities of the solid to accommodate different species so that the solid's strongest adsorbing species is preferentially removed. The last mechanism is premised on the varying diffusion rates of different species into the pore; thus, by controlling the exposure time, the faster diffusing species are preferentially removed by the solid[113].

Some characteristics are relevant for an efficient adsorbent material, such as adsorption capacity and selectivity, adsorbate uptake kinetics, renewability, low or zero solubility, no tendency to undesirable chemical reactions, compatibility with operating conditions, and low cost[114] how the solid acts both in equilibrium and kinetically are one of the signs of success or

failure of the adsorption process. This makes the material's porosity one of the essential variables for an adsorbent[113].

A solid can even have a good capacity, but if the kinetics are slow, it is not a good choice since the adsorbent molecules take a long time to reach the particle's interior. In contrast, a solid with low capacity but fast kinetics is also not a good choice since a large amount of solid is needed for a given performance. Thus, a promising adsorbent can combine a good adsorption capacity and kinetics. The solid must have a reasonably high surface area or micropore volume ($d < 2$) and a relatively large pore network to transport molecules to the interior to satisfy this combination. Some materials used as adsorbents are alumina, activated carbon, silica gel, resin, graphene, and many others[113].

The pH is one factor that influences the adsorption process since it interferes with the dissociation of functional groups present in the active sites of the adsorbent and electrostatic interaction[115]. Another factor is the temperature because it directly affects the agitation of the molecules, influencing the forces of attraction and repulsion between the adsorbate and the adsorbent, changing the adsorption capacity of the adsorbent[116].

In addition, there is also the influence of the granulometry of the adsorbent since the smaller the dimensions of the particles, the greater the total surface area exposed to adsorption. And finally, the last factor is the pore diameter, intervening in the solute's ability to reach the active site to be adsorbed[113].

2.4.3 GEOPOLYMER AS ADSORBENT

Many materials are used as adsorbents to remove heavy metals, dyes, emerging contaminants, and undesirable components in general[71]. However, due to their high surface area, stability, and durability[117], the most widely used adsorbents, activated carbons, have limitations for large-scale use because of their expensive synthesis and difficulty of regeneration[118]. Thus, the search for an efficient, environmentally friendly, economical, and efficient adsorbent is constantly expanding[71].

GPs are a promising category of porous aluminosilicate materials used as adsorbents for wastewater treatment[71]. These eco-friendly materials have attractive advantages, such as low cost, high efficiency, simple production, and readily scalable characteristics[119]. Moreover, characteristics that favor their use as adsorbents include high surface area, high Al_2O_3/SiO_2

ratio, high amorphous content, chemical stability, high porosity, and high capacity of cation exchange[120].

In addition, geopolymer manufacturing allows for the reuse of industrial and agricultural waste that would be discarded (FA, slag, and rice hulls), fostering a circular economy[121]. Because it uses minerals of geological origin, the process becomes green and environmentally friendly[85].

These factors have been a compliment in developing and researching GPs for researchers who focus on raw material recovery and not using new natural resources[122]. Using GPs in their various areas of activity allows cleaner production systems in manufacturing industries, bringing a considerable reduction in industrial, agricultural, and municipal waste[85].

Some examples in the literature show the effectiveness of GPs as adsorbents in wastewater treatment, such as biomass FA GPs for methylene blue removal[78], GPs for adsorption of lead ion[123], GPs for adsorption of radioactive iodide anions[124] and GPs adsorbent for copper ion removal from wastewater[125]. Table 4 shows more examples of adsorbent GPs, their adsorbates, and some of their characteristics.

Table 4: Examples of Adsorbent Geopolymers.

Ref.	Precursor	Alkaline activator	Curing Conditions	Adsorbate	Adsorption capacity (mg/g)
[126]	Fly ash	NaOH	72 h at 40 °C	Cadmium (Cd^{2+})	26.25
[127]	Fly ash and slag	NaOH (8 M)	24 h at 80 °C/24 h hydrothermal treatment at 90 °C	Cesium (Cs^{+})	15.24
[128]	LD slag	NaOH (10 M)	72 h at 25 °C	Nickel (Ni^{2+})	85.29
[129]	Metakaolin	NaOH	48 h at 80 °C	Manganese (Mn^{2+})	73.30
[78]	Biomass fly ash	NaOH	24 h at 40 °C	Methylene blue	15.40
[130]	Biomass fly ash	NaOH (10 M)	24 h at 40 °C/27 days at room temperature	Methylene blue	30.10

3 OBJECTIVES

This work aims to develop GPs using a by-product of MSW incineration as a precursor (FA), to characterize these produced materials and to evaluate their performance as adsorbents for wastewater treatment.

3.1 SPECIFIC OBJECTIVES

- Characterize the MSW fly ash obtained from an incineration plant;
- Developing a Design of Experiment for the optimized production of geopolymer;
- Produce and characterize GPs;
- Apply the GPs to test them as adsorbents in treating model wastewater containing gallic acid as a standard solution.

4 MATERIALS AND METHODS

4.1 REACTANTS AND EQUIPMENTS

4.1.1 REACTANTS

- Fly ash, provided by SOGAMA;
- Aluminum oxide (Al_2O_3 - 99.7%), provided by Thermo Scientific;
- Sodium Hydroxide pearls (NaOH - 98%), provided by Labkem;
- Sodium Silicate (Na_2SiO_3 - Na_2O = 10.6% and SiO_2 = 26.5%), provided by Fisher Chemical;
- Gallic Acid ($C_6H_2(OH)_3COOH$ – 98%), provided by EMD Millipore Corporation;
- Distilled water.

4.1.2 EQUIPAMENTS

- Magnetic stirrer;
- MultiMix D with thermal bath;
- Oven;
- HPLC;
- UV-Vis;
- pHmeter;
- Sieves.

4.2 METHODS

4.2.1 DESIGN OF EXPERIMENTS

The response surface method (RSM) is a proper experimental design that applies statistical and mathematical techniques to optimize the investigated variables. This methodology evaluates the impact of independent variables (x_1, x_2, ..., x_n) and their combinations, establishing an association between the variables and responses (y_1, y_2, ..., y_n) through a quadratic polynomial equation (Eq. 1). The most commonly used RSM designs include the Central Composite Design (CCD), the Box-Behnken design (BBD), and the three-level factorial design[131].

$$y = \beta_0 + \sum_{i=1}^{k} \beta_i x_i + \sum_{i=1}^{k} \beta_{ii} x_i^2 + \sum_{i=1}^{k-1} \sum_{j=2}^{k} \beta_{ij} x_i x_j \quad (1)$$

Where y is the output response, β is the regression coefficient estimated from the experimental data, k is the number of experimental parameters, x_i, and x_j are the variables that represent the evaluated parameters.

The Box-Behnken Design (BBD) has been employed in the present study to optimize the synthesis of GPs materials. The Box-Behnken design uses a design matrix consisting of a combination of three levels (-1, 0, +1) for each independent variable. The design places points on the midpoints of the edges of the cubic design region and points in the center to generate a set of experimental data that can be used to model the response surface and optimize the process parameters. It utilizes the twelve center edge nodes and the three center nodes to fit a second-order equation, resulting in 15 experiments. Figure 8 shows a scheme that represents this design[132].

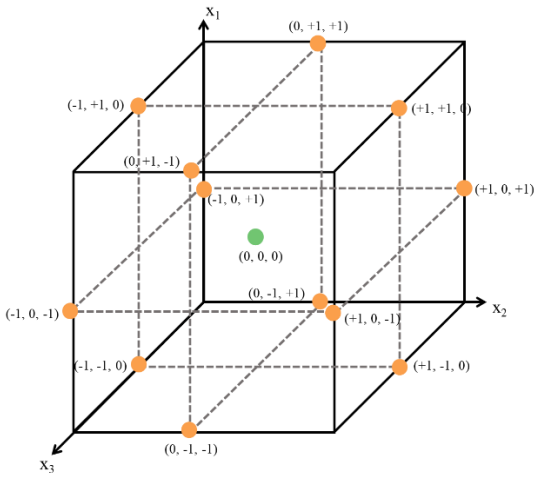

Figure 8: BBD for 3 independent variables.

Three parameters that have been previously identified to influence this process are considered: Si/Al mass ratio[133–135], NaOH molar concentration (M)[135,136], and Na_2SiO_3/NaOH weight ratio[137,138]. Each factor was tested at three levels of component content, high (1), medium (0), and low (-1). Table 5 shows the ranges and experimental values of the independent variables that were considered for the design.

Table 5: Experimental variables and their levels used in the BBD.

Factor	Original Factor (x)	Levels		
		-1	0	1
Si/Al	x_1	1.50	2.00	2.50
NaOH (M)	x_2	5.00	7.50	10.0
Na_2SiO_3/NaOH	x_3	1.00	1.75	2.50

The design was created and analyzed using R-Studio, which was used for design conception, mathematical modeling, graphical and statistical treatment of the results, and optimization. The response values recorded for the GPs is removal efficiency (%) for gallic acid value Table 6 displays the experimental design matrix.

Table 6: Box–Behnken design layout.

Experiment		Coded Factors		
Logical	Random	x_1	x_2	x_3
1	8	-1	-1	0
2	13	1	-1	0
3	10	-1	1	0
4	12	1	1	0
5	11	-1	0	-1
6	9	1	0	-1
7	7	-1	0	1
8	3	1	0	1
9	5	0	-1	-1
10	15	0	1	-1
11	4	0	-1	1
12	6	0	1	1
13	1	0	0	0
14	2	0	0	0
15	14	0	0	0

4.2.2 GEOPOLYMER SYNTHESIS

The MSWI fly ash used in this study was obtained from Sogama, an environmental complex in Cerceda, Spain, responsible for managing most of the MSW in the Galician region[139].

Fifteen GPs were synthesized using the Design of Experiment approach, with each sample utilizing an initial FA mass of 10 g. The reactants were mixed uniformly by hand in a beaker,

and the resulting homogenous geopolymer paste was molded into cubic forms measuring 45 x 45 x 45 mm. The samples were then cured at 40 °C for 24 hours in an oven. The exact amount of each component in each test is shown in Table 7.

Table 7: Reagent quantity for the formulation of GPs.

Experiment		Factors			Na_2SiO_3 (g)	NaOH (g)	Al_2O_3 (g)	H_2O (mL)
Logical	Random	Si/Al	NaOH (M)	Na_2SiO_3/NaOH				
1	8	-1	-1	0	4.00	2.29	0.18	11.2
2	13	1	-1	0	9.55	5.46	-	26.74
3	10	-1	1	0	4.00	2.29	0.18	5.60
4	12	1	1	0	9.55	5.46	-	13.37
5	11	-1	0	-1	4.00	4.00	0.18	13.07
6	9	1	0	-1	9.55	9.55	-	31.20
7	7	-1	0	1	4.00	1.60	0.18	5.23
8	3	1	0	1	9.55	3.82	-	12.48
9	5	0	-1	-1	5.67	5.67	-	27.78
10	15	0	1	-1	5.67	5.67	-	13.90
11	4	0	-1	1	5.67	2.27	-	11.12
12	6	0	1	1	5.67	2.27	-	5.56
13	1	0	0	0	5.67	3.24	-	10.58
14	2	0	0	0	5.67	3.24	-	10.58
15	14	0	0	0	5.67	3.24	-	10.58

4.2.2.1 GEOPOLYMERS POWDER PREPARATION

The synthesized GPs underwent various analyses and adsorption tests following the curing process. To prepare the samples for adsorption tests, the following steps were taken:

- The GPs were ground into a fine powder.
- The crushed GP was washed multiple times with distilled water and a 0.1 M hydrochloric acid solution until the pH of the solution containing the GP reached neutrality ($pH \leq 7$).
- The washed GP was then dried overnight at 40 °C.
- The dried GP was sieved to obtain particles smaller than 53 μm.
- The sieved GP was stored for further analysis and adsorption tests.

This preparation procedure ensured the samples were properly cleaned and sized for accurate and reliable analysis. Figure 9 shows the geopolymer preparation stages, from its precursor, fly ash, to its sieved form.

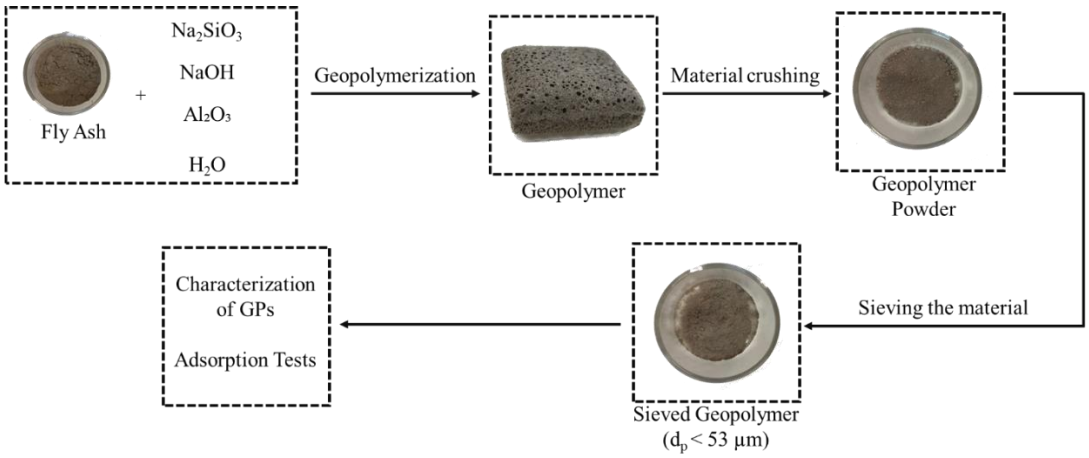

Figure 9: Geopolymer preparation phases.

4.2.3 CHARACTERIZATION OF MATERIALS

4.2.3.1 INDUCTIVELY COUPLED PLASMA OPTICAL EMISSION SPECTROSCOPY (ICP-OES)

To analyze the chemical composition of MSW fly ash, inductively coupled plasma (ICP) analysis was used. The method used for this analysis was ICP-OES, which is based on the excitation of the electron to a more active layer due to energy absorption from the atom. In ICP-OES, the energy source to move the electron is the heat of an argon plasma. This technique is highly effective in identifying and measuring various chemical elements from the sample of interest. This analysis was done at Rey Juan Carlos University – Spain.

4.2.3.2 POROSIMETRY AND SURFACE AREA

Accurately characterizing GPs' porosity and surface area is crucial for evaluating their potential as effective adsorbents. These properties of the materials were determined from N_2 adsorption-desorption isotherms at 77.35 K, using long cells with a bulb and an outer diameter of 9 mm in a Quantachrome instrument NOVA TOUCH LX^4. The outgassing process was conducted at 200 °C for 3 hours. The specific surface area (S_{BET}) was calculated by the BET method using Quantachrome TouchWin software within the range of p/p_0 0.05 – 0.35.

4.2.3.3 FOURIER-TRANSFORM INFRARED SPECTROSCOPY (FT-IR)

Fourier Transform Infrared Spectroscopy (FT-IR) was applied to analyze the chemical structure of the GPs and FA. FT-IR spectra were collected using a Perkin Elmer FT-IR spectrophotometer UATR Two infrared spectrophotometer in the wavenumber range of 450 to 4000 cm^{-1} at room temperature with solid samples. The raw data were processed using the Fourier transform to obtain the actual spectrum for further analysis.

4.2.3.4 SCANNING ELECTRON MICROSCOPY WITH ENERGY DISPERSIVE SPECTROSCOPY (SEM/EDS)

Scanning electron microscopy combined with energy dispersive spectroscopy (SEM/EDS) was conducted to investigate the morphological and microstructural features of the precursor material and GPs and identify the elements present in the samples. This analysis was done at University of Trás-os-Montes and Alto Douro.

4.2.3.5 X-RAY DIFFRACTION (XRD)

X-ray diffraction (XRD) measurements were performed on the material by depositing it on a glass sample holder and analyzing it using a diffractometer. The data were processed using HighScore Plus to obtain the material's phase identification and crystal structure information. This analysis was done at University of Trás-os-Montes and Alto Douro.

4.2.3.6 ACID-BASE CHARACTERIZATION

Determining the acid-base properties of the material is a critical factor that can significantly affect the performance of GPs as adsorbents. This analysis provides valuable information about the mechanism of adsorption and the interaction between the adsorbent and the adsorbate. Understanding the acid-base properties can give insights into the surface charge and functional groups. To evaluate this property, five distinct solutions were prepared:

- 1 L of NaCl 0.01 mol/L
- 500 mL of HCl 0.02 mol/L
- 500 mL of HCl 0.01 mol/L

- 500 mL of NaOH 0.02 mol/L
- 500 mL of NaOH 0.01 mol/L

The titration process enables the determination of the concentration of a titrated solution based on the known concentration and volume of the titrant solution. Applying this method to geopolymeric materials makes it possible to quantify the number of moles that react with the acidic or basic sites present in the material. This information provides valuable insights into the material's acid-base properties, allowing characterization of its basicity or acidity.

4.2.3.6.1 ACIDIC SITES DETERMINATION

The solid sample (0.2 g) was added to 25 mL of a 0.02 mol/L NaOH solution and mixed on a magnetic stirrer at 300 rpm for 48 hours. The resulting solution was then filtered, and a 20 mL aliquot of the recovered solution was titrated with 0.01 mol/L HCl solution using phenolphthalein as an indicator.

4.2.3.6.2 BASIC SITES DETERMINATION

0.2 g of the solid sample was added to 25 mL of 0.02 mol/L HCl solution and mixed on a magnetic stirrer at 300 rpm for 48 h. After filtration, 20 mL of the recovered solution was titrated with 0.01 mol/L NaOH solution, using phenolphthalein as an indicator.

4.2.3.6.3 POINT OF ZERO CHARGE (PZC) DETERMINATION

Nine dilutions of 0.01 mol/L NaCl were prepared in Erlenmeyer flasks. The pH of each solution was adjusted to values ranging from 4 to 12 by adding 0.02 mol/L NaOH or HCl. To study the effect of pH on the material's performance as an adsorbent, 0.15 g of the solid sample was added to each solution, which was then stirred on a magnetic stirrer at 300 rpm and 25 ºC for 24 h. After filtering the solutions, their pH was measured. The final pH values were plotted on the y-axis and the corresponding initial values on the x-axis. A correlation was established between these two values, and an identity curve was generated on the graph. The intersection point between the pH value curves and the identity curve represents the pH at the point of zero charge (pHpzc).

4.2.4 ADSORPTION TESTS

4.2.4.1 ADSORPTION KINETICS

A series of procedures were performed to evaluate the adsorption kinetics of the geopolymer powders for gallic acid.

- The solution containing 50 mg/L of gallic acid was prepared with a volume of 100 mL;
- A geopolymer mass of 0.25 g was added to the solution, resulting in a concentration of 2.5 g/L of adsorbent;
- The solution was agitated on a magnetic stirrer at 300 rpm while maintaining a constant temperature of 50 °C for 8 hours;
- At 8 different time intervals (0, 15, 30, 60, 120, 240, 360, and 480 minutes), aliquots of 2 mL have withdrawn from the solution.

After completing the adsorption tests, the solutions were vacuum filtered to separate the adsorbent from the solution. The adsorbent was collected, dried at 40 °C for 24 hours, weighed, and stored. The pH of the filtrates was measured to evaluate any changes in acidity or basicity during the adsorption process.

Adsorption capacity q (mg/g) was determined with Eq. 2, while the GPs' removal efficiency E (%) was calculated using Eq. 3.

$$q = \frac{(C_0 - C_e) \times V}{m} \quad (2)$$

$$E = \frac{(C_0 - C_e)}{C_0} \times 100\% \quad (3)$$

Where C_0 (mg/L) is the initial concentration of the pollutant (gallic acid), C_e (mg/L) is the concentration in the liquid phase of the pollutant at the equilibrium time, V (L) is the volume of the pollutant solution, and m (g) is the mass of adsorbent.

4.2.4.1.1 KINETIC MODELS

The study of adsorption kinetics provides essential information about the interactions between the adsorbent and the adsorbate and the mechanisms of mass transfer from the adsorbate to the liquid-solid interface.

Several kinetic models have been proposed for solid-liquid adsorption. This study employed three kinetic models: the pseudo-first-order model, the pseudo-second order, and the intraparticle diffusion model. The mathematical expression for the pseudo-first-order model is given by Equation 4[140].

$$q_t = q_e(1 - e^{-k_1 t}) \quad (4)$$

Where q_t is the adsorption capacity (mg/g) at a time t (min), q_e is the adsorption capacity at equilibrium (mg/g), and k_1 is the adsorption rate kinetic constant of the pseudo-first-order model (min^{-1}).

The pseudo-second-order model can be mathematically represented by Equation 5[140].

$$q_t = \frac{q_e^2 k_2 t}{1 + q_e k_2 t} \quad (5)$$

Where q_t and q_e are the adsorption capacity (mg/g) at a time t (min) and equilibrium, respectively, and k_2 is the adsorption rate kinetic constant of the pseudo-second-order model (g mg^{-1} min^{-1}).

Equation 6 represents the mathematical formulation of the intraparticle diffusion model.

$$q_t = k_{id} t^{1/2} + I \quad (6)$$

Where q_t is the adsorption capacity (mg/g) at a time t (min), k_{id} is the intraparticle diffusion rate constant (mg/(g·$min^{0.5}$)), and I (mg/g) is the intercept.

4.2.4.2 EQUILIBRIUM ISOTHERMS

To construct the equilibrium isotherms, some steps were followed.

- Preparation of 50 mL solutions of gallic acid with 5 different concentrations: 10, 30, 50, 75, and 100 mg/L;
- A geopolymer mass of 0.125 g was added to the solution, resulting in a concentration of 2.5 g/L of adsorbent;
- The solution was agitated on a magnetic stirrer at 300 rpm while maintaining a constant temperature of 50 °C for 6 hours;
- At the final time, a 2 mL aliquot was collected.

4.2.4.2.1 EQUILIBRIUM ISOTHERMS MODELS

Adsorption isotherms are essential for studying the equilibrium stage of adsorption and can provide valuable information about the interactions between the adsorbent and the adsorbate. This information can be used to optimize the use of adsorbents, select the most suitable adsorbent, and predict the performance of the adsorption system[141].

Two commonly used isotherms for solid-liquid systems will be evaluated: Langmuir and Freundlich. The Langmuir isotherm is based on the assumption of monolayer coverage of non-interacting molecules[141]. The expression that represents this model is given by Equation 7.

$$q_{eq} = \frac{q_{max} K_L C_{eq}}{1 + K_L C_{eq}} \tag{7}$$

Where q_{eq} is the adsorption capacity at equilibrium (mg/g), q_{max} is the maximum adsorption capacity of the adsorbent (mg/g), C_{eq} is the GA equilibrium concentration (mg/L), and K_L is the Langmuir adsorption constant (L/mg).

By using the K_L parameter derived from the Langmuir isotherm, another parameter known as R_L (Equation 8) can be calculated. This parameter serves as an indicator of the affinity of the solute for sites on the adsorbent material. When $R_L = 0$, the adsorption process is considered irreversible. If $0 < R_L < 1$, the process is considered favorable to adsorption. A value of RL = 1 signifies a linear process, while $R_L > 1$ indicates an unfavorable adsorption process [78].

$$R_L = \frac{1}{1 + K_L C_0} \tag{8}$$

R_L is the indicator of the affinity of the solute, K_L is the Langmuir adsorption constant (L/mg), and C_0 is the initial concentration of gallic acid (mg/L).

The Freundlich isotherm model, in contrast, is interpreted as a model for sorption onto a heterogeneous surface that contains sites with varying affinities[78]. Equation 9 shows the representation of this model.

$$q_{eq} = K_F C_{eq}^{1/n_F} \tag{9}$$

Where q_{eq} is the adsorption capacity at equilibrium (mg/g), C_{eq} is the GA equilibrium concentration (mg/L), K_F is the Freundlich constant (L/g), and n_F is the dimensionless Freundlich constant related to the intensity of adsorption, values in the range 1 to 10 represent favorable adsorption conditions.

4.2.5 ANALYTICAL METHOD

4.2.5.1 HPLC

HPLC (high-performance liquid chromatography) was used to identify the presence of gallic acid in samples collected in the adsorption test. The Ultra BiPh 5µm column (150 mm x 2.1 mm) was used for this analysis, along with a mobile phase comprising 5% of acetonitrile and 95% phosphoric acid. The isocratic system was run at a flow rate of 0.3 mL/min, and gallic acid was detected at a wavelength of 277 nm.

Before analyzing the gallic acid solution obtained from the adsorption tests, a calibration curve was constructed within the 1-50 mg/L reading range. The calibration curve exhibited a high level of accuracy, as indicated by the excellent fit obtained with an R^2 value of 1, determined through linear regression analysis. Figure 10 presents a graphical representation of the calibration curve generated for the analyses.

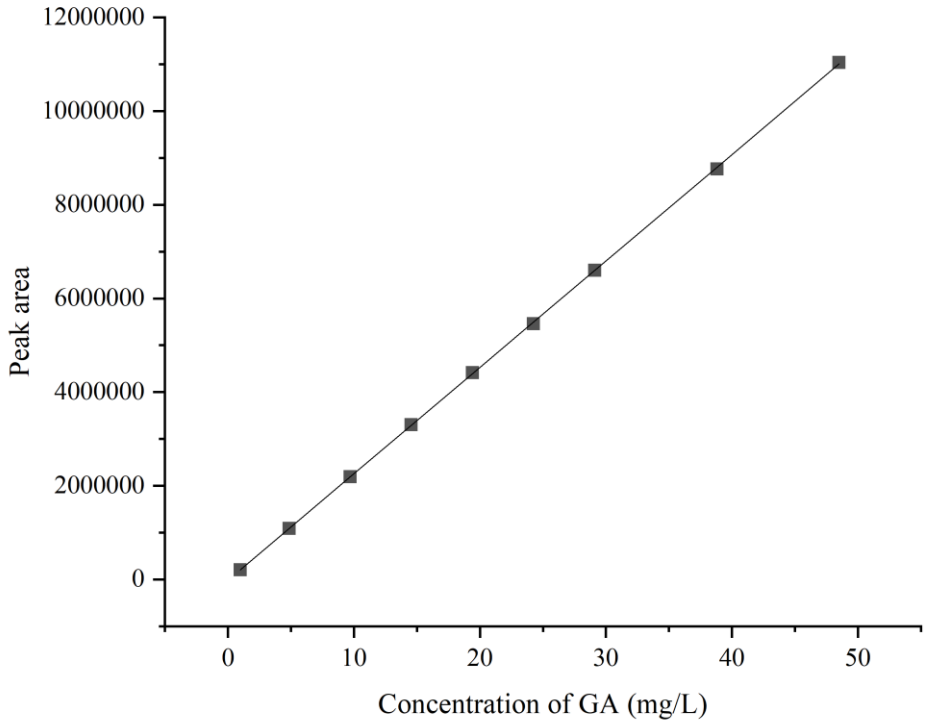

Figure 10: Calibration curve for gallic acid measurements.

5 RESULTS AND DISCUSSION

5.1 RESPONSE SURFACE ANALYSIS

As mentioned above, the RSM was utilized to investigate and analyze the relationship between the response and independent variables. Table 8 presents the removal efficiency of GA for each geopolymer produced as determined by the experimental design conducted in this study. The removal efficiency indicates the percentage of gallic acid effectively removed by the geopolymer.

Table 8: BBD experimental results.

Experiment		**Factors**			**Response**
		x_1	x_2	x_3	y_1
Logical	**Random**	**Si/Al**	**NaOH (M)**	**Na_2SiO_3/NaOH**	**Removal (%)**
1	8	1.50	5.00	1.75	97.17
2	13	2.50	5.00	1.75	**99.51**
3	10	1.50	10.0	1.75	97.13
4	12	2.50	10.0	1.75	**99.07**
5	11	1.50	7.50	1.00	98.11
6	9	2.50	7.50	1.00	**99.72**
7	7	1.50	7.50	2.50	97.14
8	3	2.50	7.50	2.50	**99.30**
9	5	2.00	5.00	1.00	98.71
10	15	2.00	10.0	1.00	98.67
11	4	2.00	5.00	2.50	98.59
12	6	2.00	10.0	2.50	98.97
13	1	2.00	7.50	1.75	98.61
14	2	2.00	7.50	1.75	97.63
15	14	2.00	7.50	1.75	98.08

The results presented in Table 8 allow the analysis of the relationship between the removal efficiency and the proposed three factors: Si/Al ratio, NaOH concentration (M), and Na_2SiO_3/NaOH ratio. Among these factors, the Si/Al ratio influences the response significantly. This can be observed by considering the highest removal efficiency values (shown in bold), which correspond to geopolymer samples with a Si/Al ratio of 2.5, the highest value used in the experiment design. On the other hand, all the lowest removal efficiency values (shown in underline) are associated with a Si/Al ratio of 1.50, the minimum value used in the experiment design.

The experimental data suggest a directly proportional correlation between the Si/Al ratio and the efficiency of gallic acid removal by the produced GPs. This observation aligns with the existing literature[76], which indicates that a higher Si/Al ratio corresponds to a larger surface area of the geopolymer. As a result, active sites for gallic acid adsorption are more available. The more significant number of active sites facilitates the removal of the pollutant, leading to higher removal percentages.

Contour plots were generated using the R-Studio tool to visualize the relationship between the independent variables (Figure 11). In each contour plot, one factor was maintained constant at its midpoint value, while the other two factors varied from their minimum to maximum range. This approach explains how changes in the independent variables affect the response variable by examining the contours of the response levels at different combinations of the variable factors.

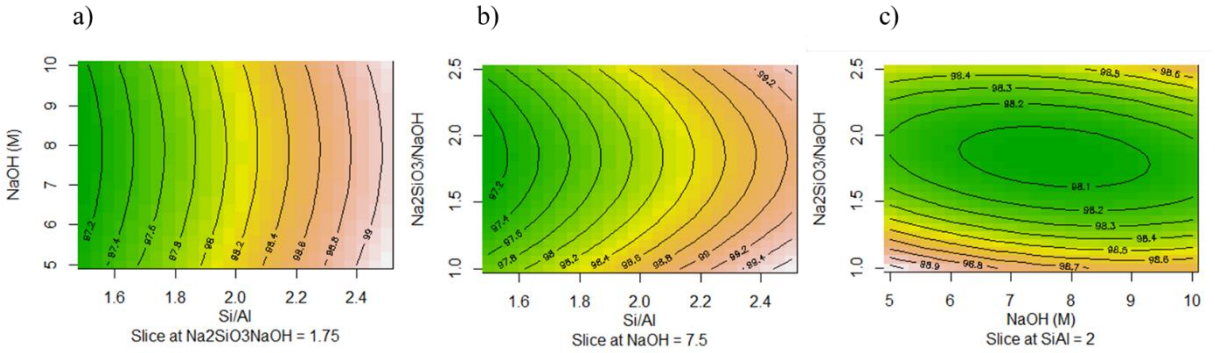

Figure 11: Contour graphs of GA removal: a) NaOH as a function of Si/Al; b) Na_2SiO_3/NaOH as a function of Si/Al, and c) Na_2SiO_3/NaOH as a function of NaOH.

In Figure 11a, where the Na_2SiO_3/NaOH factor is held constant equal to 1.75, and the other two factors are varied, it is evident that the removal efficiency increases with increasing Si/Al ratio, as expected. Furthermore, the curved nature of the lines suggests a nonlinear relationship between the molar concentration of NaOH and the Si/Al ratio.

In Figure 11b, when the factor x_2 is 7.5 and the others are varied, it can be observed that the percent removal increases with an increase in the Si/Al ratio. Additionally, there is no apparent linear relationship between the factor x_1 (Si/Al ratio) and the factor x_3, indicating that their interaction does not follow a simple linear trend.

In Figure 11c, fixing the Si/Al ratio equal to 2, it can be noted that increasing the Na_2SiO_3/NaOH ratio initially leads to decreased removal efficiency. However, when the

Na_2SiO_3/NaOH ratio reaches approximately 2, further increases in this ratio increase removal efficiency. It is observed that, in general, increasing the NaOH concentration leads to a decrease in removal efficiency when combined with Na_2SiO_3/NaOH ratios less than 2. However, for ratios greater than 2, increasing the NaOH concentration increases removal efficiency.

The exact contour plots in the software were generated in three dimensions and are shown in Figure 12. These plots provide visual representations in 3D of the relationship between the independent variables and the response variable.

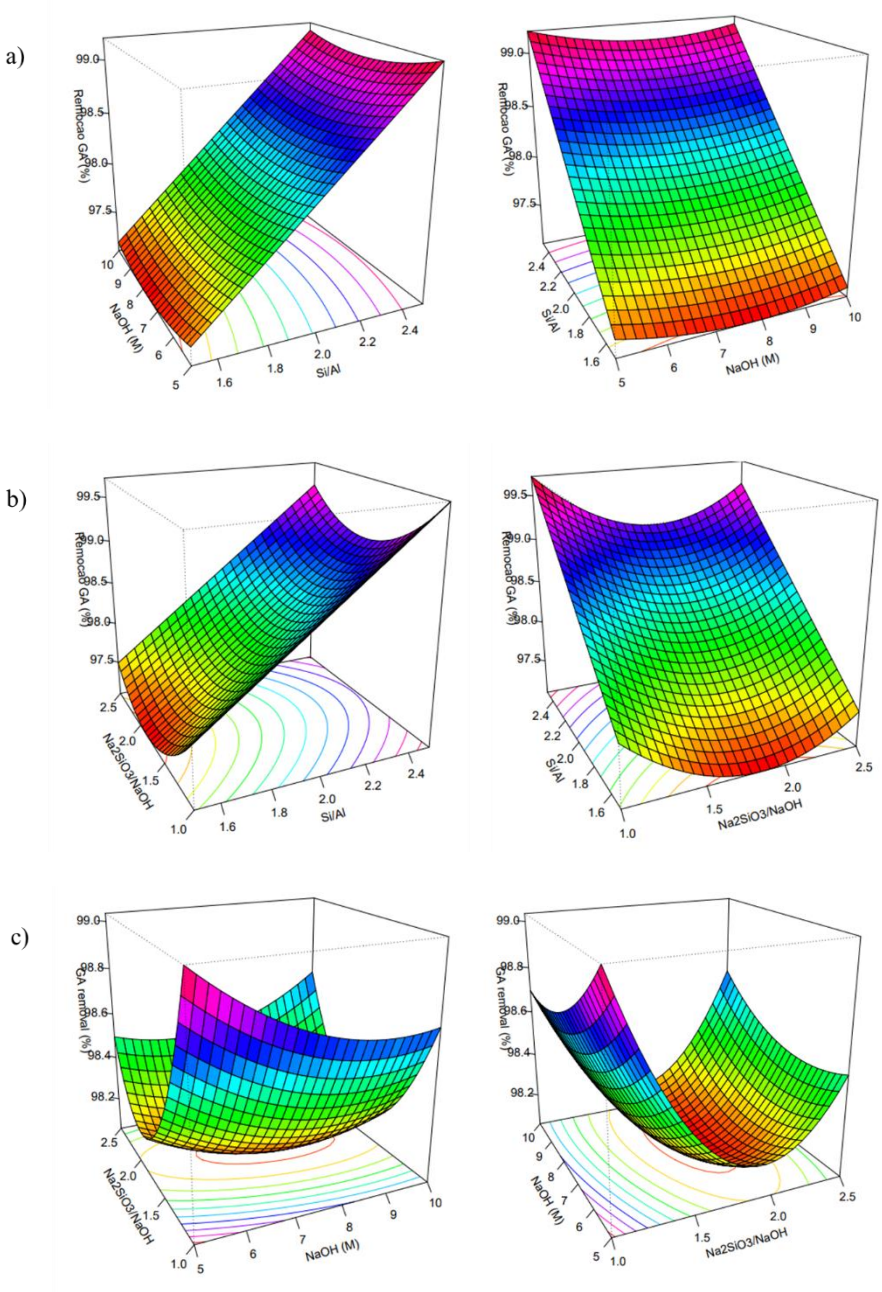

Figure 12: 3D contour graphs: a) fixing Na_2SiO_3/NaOH, b) fixing NaOH (M), and c) fixing Si/Al.

In R-Studio, the statistical analyses were performed using the equation presented in Equation 10. This equation is a modified form of Equation 1, adapted for programming in the software used.

$$Y = FO(x_1, x_2, x_3) + TWI(x_1, x_2) + TWI(x_1, x_3) + TWI(x_2, x_3) + PQ(x_1, x_2, x_3) \quad (10)$$

Where *Y* is the output response, x_1, x_2, and x_3 are the variables that represent the parameters, the *FO* is the linear and individual correlation of terms, *TWI* is the dual relationship between variables, and *PQ* is the quadratic relationships between terms.

After performing the initial analysis using Equation 10, it was evident that adjustments were necessary to improve the results obtained since the adjusted R^2 was 0.72. To improve this value, the p-values of each factor analyzed were evaluated, with the ideal p-value being less than 0.05[138]. The factors that presented higher p-values were removed from the equation to increase the model's predictive ability and statistical significance; the resulting equation is Equation 11. This process aimed to refine the equation and ensure that only the most influential factors were included, thus improving the model's overall accuracy.

$$Y = FO(x_1, x_2, x_3) + TWI(x_2, x_3) + PQ(x_2, x_3) \quad (11)$$

With the equation in this form, the results obtained by statistical analysis are shown in Table 9.

Table 9: The influence of model coefficients linking response to a variable.

	Estimate	**Std. Error**	**t value**	**Prob>|t|**
x_1	0.974	0.138	7.066	1,06E-01
x_2	-0.037	0.138	-0.272	0.792
x_3	-0.139	0.138	-1.007	0.343
x_2:x_3	0.130	0.195	0.667	0.523
x_2^2	0.126	0.202	0.623	0.551
x_3^2	0.538	0.202	2.662	0.029
R^2	**adj R^2**	**p-value**		
0.880	0.800	0.002		

The model's fitted values produced an R^2 value of 0.800, higher than the previous equation's. However, this value is still considered unsatisfactory, suggesting that some experimental data does not align well with the model used. This disparity indicates a discrepancy between the predicted values of the model and the actual experimental results. On the other hand, the p-value of 0.002 was considered satisfactory, indicating that at least one of

the predictor variables in the model presents a significant relationship with the response variable. Consequently, the regression model demonstrates statistical significance in explaining the variability observed in the response variable.

Furthermore, in Table 9, it is possible to observe the impact of the variables examined on the measured response. The estimated coefficient for each factor means the magnitude of the impact on the final response resulting from variations in the respective variables. For example, a coefficient value of 0.974 for variable x_1 indicates that, on average, a one-unit increase in x_1 is associated with an average 0.974 unit increase in the response variable, assuming all other variables stay unchanged. Similarly, the negative coefficients of variables x_2 and x_3 indicate a negative relationship between these variables and the analyzed response. This means that as the values of x_2 and x_3 increase, the response variable is expected to decrease.

Based on the provided coefficients, it is evident that the variable with the most significant influence on the responses is x_1, representing the Si/Al ratio. Additionally, the squared term of x_3, denoting Na_2SiO_3/NaOH, significantly impacts the responses.

The observations regarding the t-values and p-values further confirm the influence of the factors on the responses. A higher t-value corresponds to a lower p-value; for a term to be considered statistically significant, the p-value should be less than 0.05. By evaluating the p-values for each factor, it can be reaffirmed that both x_1 (Si/Al ratio) and x_3^2 (Na_2SiO_3/NaOH) significantly affect the geopolymer's efficiency of gallic acid removal. Considering only the independent variables that significantly affect the response variable, the equation analyzed is as shown in Equation 12.

$$Y = FO(x_1) + PQ(x_3) \tag{12}$$

It is important to note that analyzing only the removal efficiency is not sufficient to evaluate the performance of an adsorbent, as it only considers the initial and final concentration of the adsorbate in the fluid phase, neglecting other factors involved in adsorption, such as the mass of the adsorbent used and the volume of the solution. Additionally, it does not take into account other properties of the adsorbents.

Therefore, five GPs were chosen for a more in-depth study of their characteristics as adsorbents. The selected GPs that are highlighted in Table 8 are GP-2, as it represents one of the central points in the experimental design; GP-6, which exhibited an intermediate removal

efficiency; GP-10 and GP-11, which showed the lowest removal efficiencies; and GP-13, which demonstrated one of the highest removal efficiencies.

5.2 CHARACTERIZATION OF MATERIALS

5.2.1 ICP-OES

Fly ash chemical composition and proportions were determined using the ICP-OES test. The Si/Al mass ratio is equal to 1.27 in FA. The obtained values are presented in Table 10.

Table 10: Composition and content of FA (wt %).

	Ca	**Si**	**Al**	**K**	**Fe**	**Mg**	**Zn**	**Cu**	**Mn**
FA	27.47	12.17	9.60	2.92	2.10	1.87	0.43	0.15	0.08

5.2.2 POROSIMETRY AND SURFACE AREA

Table 11 presents the textural properties results for FA and GPs 2, 6, 10, 11, and 13. The data shows a significant increase in the surface area of all the GPs compared to the precursor material, which is attributed to their higher porosity. In general, the surface area of geopolymers is three times larger than that of their precursor.

Moreover, the geopolymerization process led to an increase in the total pore volume, which is generally 6 times higher than FA, indicating the role of this process in enhancing pore formation within the geopolymer matrix[142]. It is worth noting that the average pore size of the GPs generally did not show significant changes compared to the FA. However, GP-13 exhibited an average pore size of 2.3 nm, which was notably different from the other GPs and the other analyzed parameters.

Table 11: Textural properties analysis of FA and GPs adsorbents.

	FA	**GP-2**	**GP-6**	**GP-10**	**GP-11**	**GP-13**
BET surface area (m^2/g)	11	35	30	30	30	61
Total pore volume (cm^3/g)	0.0137	0.0669	0.0619	0.0773	0.0773	0.110
Average pore width (nm)	1.8	1.8	1.8	1.8	1.8	2.3

The surface area results for GP-2, GP-6, GP-10, and GP-11 are comparable to those shown by Syial et al.[142], who produced a geopolymer using the same precursor. The surface area obtained in that study was 31.873 m²/g, while in this study, it was found to be 35 m²/g for GP-2 and 30 m²/g for GP-6, GP-10 and GP-11. The higher surface area of GP-13, which was found to be 61 m²/g, is comparable to the result obtained by Li et al.[140], who observed a geopolymer prepared using FA as a precursor with a surface area of 56.000 m²/g. This indicates that the geopolymerization process used in this study effectively produced a high surface area material.

Furthermore, it is notable that GP-13 exhibited a significantly more significant increase in pore volume compared to the other GPs. In fact, the pore volume of GP-13 was approximately ten times greater than that of FA. This result aligns with previous studies that reported a positive correlation between Si/Al ratio and pore volume[80] and a negative correlation between NaOH concentration and pore volume[143]. Thus, the high Si/Al ratio (2.5) and low NaOH concentration (5M) of GP-13 probably contributed to its substantially larger pore volume than the other GPs.

5.2.3 FOURIER-TRANSFORM INFRARED SPECTROSCOPY (FT-IR)

Functional groups in FA and GPs were analyzed using the FT-IR method. Figure 13 presents the results obtained through this method. The comparison between the spectra of the geopolymer and FA samples reveals some differences in the peak intensities and positions. It is important to note that higher transmittance percentages indicate lower amounts of functional groups[144].

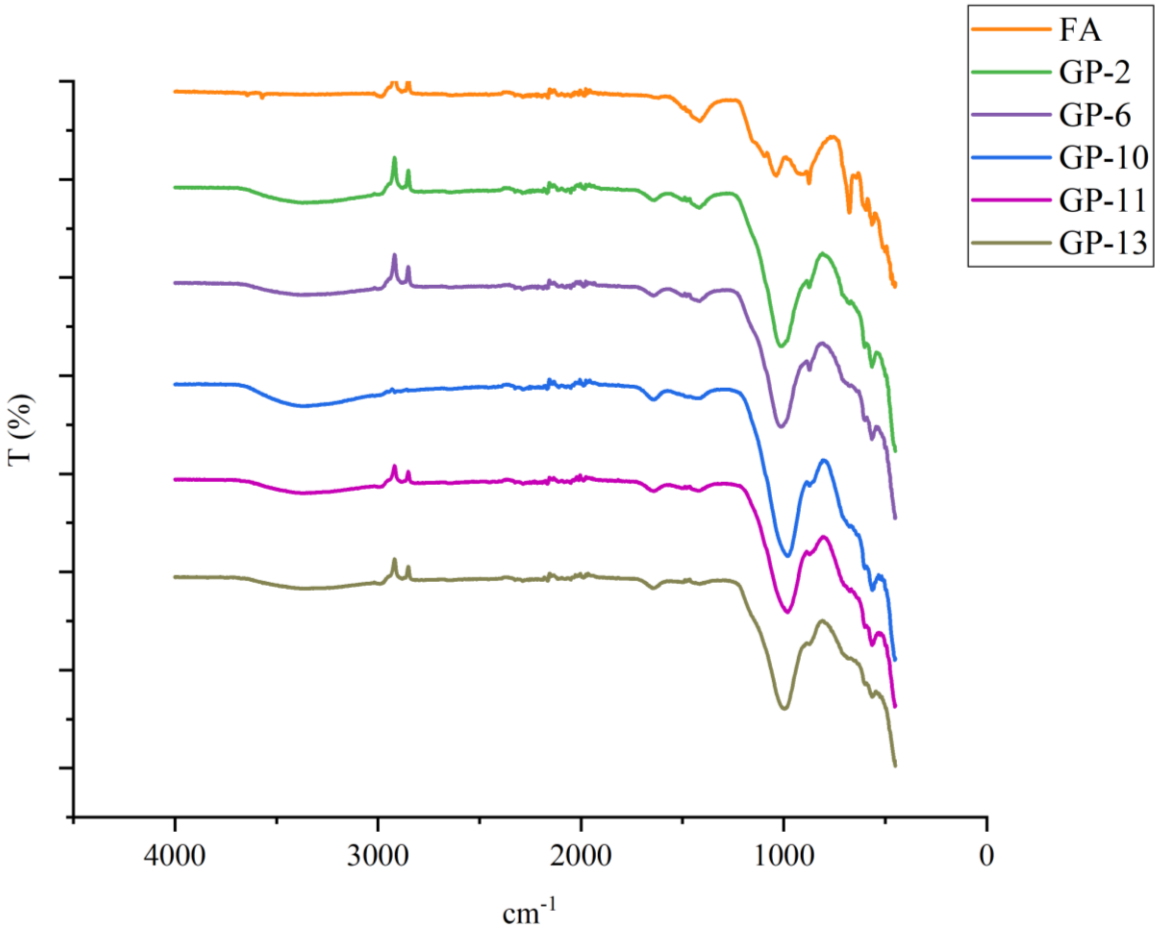

Figure 13: FT-IR spectra of FA and GPs.

In all the analyzed geopolymer samples, a peak of about 3400 cm^{-1} was observed, indicating the presence of hydroxyl groups (-OH) in the geopolymer matrix. The narrow band at about 1600 cm^{-1} was also observed, suggesting the presence of H-O-H from water hydroxyl groups[144,145]. In the spectra of both FA and geopolymer samples, a peak at approximately 1400 cm^{-1} followed by a weak band at nearly 870 cm^{-1} was observed, indicating the presence of C-O bending vibrations for CO_3^{-2} group[145]. It is believed that these bands formed due to the carbonation of the surface by atmospheric CO_2[146].

The peak observed at 1037 cm^{-1} in the FA spectrum corresponds to the asymmetric stretching vibrations of Si-O-T (T-tetrahedral Al or Si). However, in all geopolymer samples, this peak was in a lower wavenumber range of 1000-980 cm^{-1} while increasing in intensity, indicating the synthesis of GPs. The shifts in the main peak observed during comparing FA and geopolymer spectra are attributed to breaking and forming bonds during geopolymerization. Specifically, moving the main peak to lower wavenumbers suggests changes in the length and

angle of the Si-O-Si bonds in the gel[142]. Furthermore, peaks around 580-560 cm^{-1} in the geopolymer samples are attributed to the ring vibrations of Si-O bonds in the silicate network[145].

In a previous study conducted by Syial et al.[142], FT-IR analysis was performed on GPs prepared from FA to use as adsorbents. The analysis revealed specific bands in the spectrum that indicate certain molecular groups. In particular, bands around 3400 cm^{-1} and 1600 cm^{-1} were observed, corresponding to the H-O-H and -OH groups. In addition, the presence of Si-O-T bonds (where T represents Al or tetrahedral Si) was indicated by bands at 1058 cm^{-1} for FA and 1004 cm^{-1} for the geopolymer. The reduction in the intensity of this band in the geopolymer spectrum suggests a characteristic change associated with geopolymerization. These results agree with the findings of the current work, and a comparison of the spectrograms is presented in Figure 14.

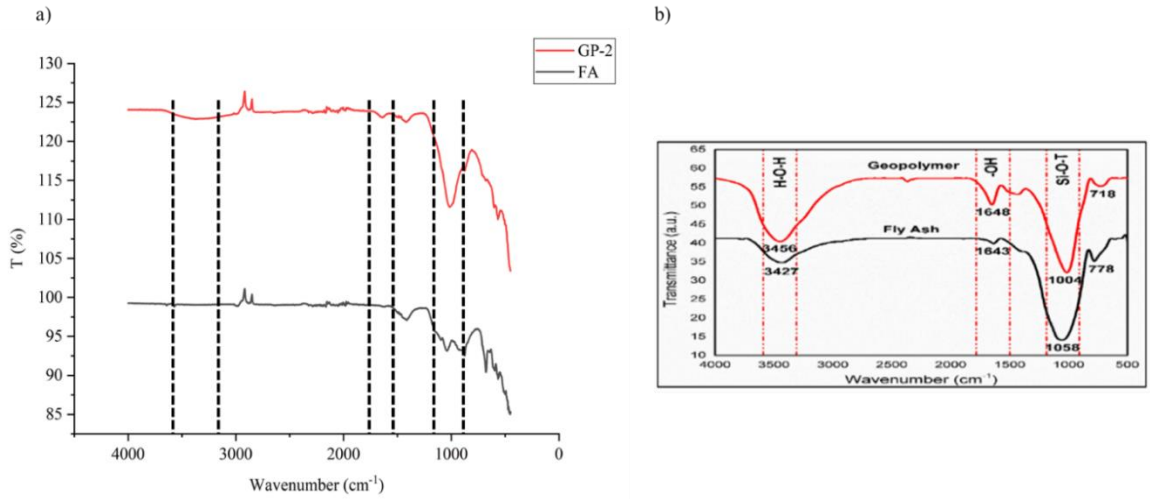

Figure 14: FT-IR spectra of a) present study and b) Syial et al.[142].

5.2.4 SCANNING ELECTRON MICROSCOPY WITH ENERGY DISPERSIVE SPECTROSCOPY (SEM/EDS)

The morphology of the FA and GP samples was studied using SEM/EDS microscopy. The results obtained from the EDS analysis are consistent with those obtained from the ICP analysis (Table 10), which show calcium as the primary component of the FA. Moreover, it is possible to observe the increase in silicon, aluminum, and oxygen content in all the GPs due to the geopolymerization process, as shown in Figure 15.

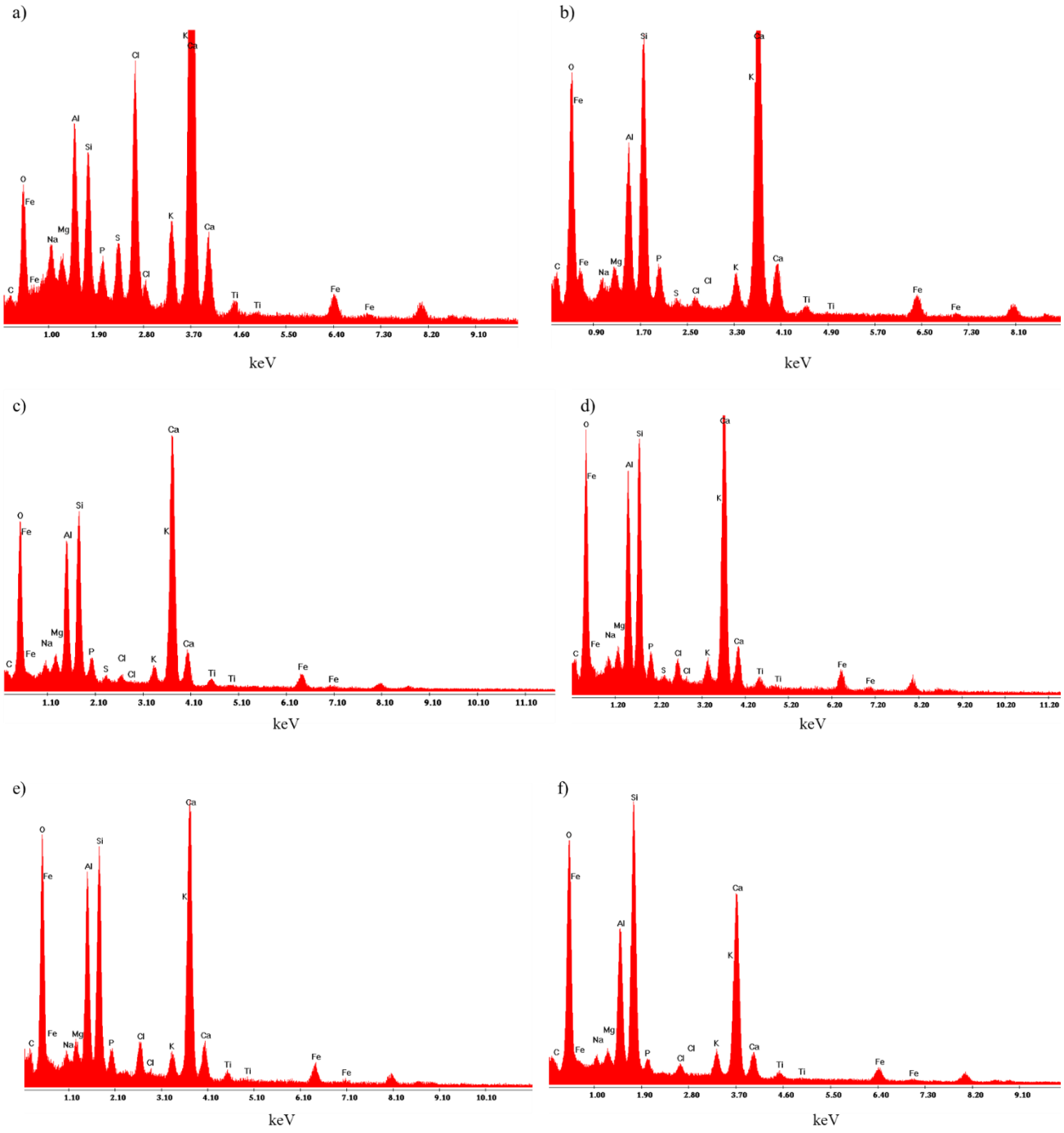

Figure 15: EDS analysis of a) FA, b) GP-2, c) GP-6, d) GP-10, e) GP-11 and f) GP-13.

The structure of FA (Figure 16) is intricate and multifaceted, characterized by an amalgamation of independent and agglomerated particles that appear round and spherical but vary in size and shape. These particles are often interspersed with interconnected pores, further complicating the overall structure[147].

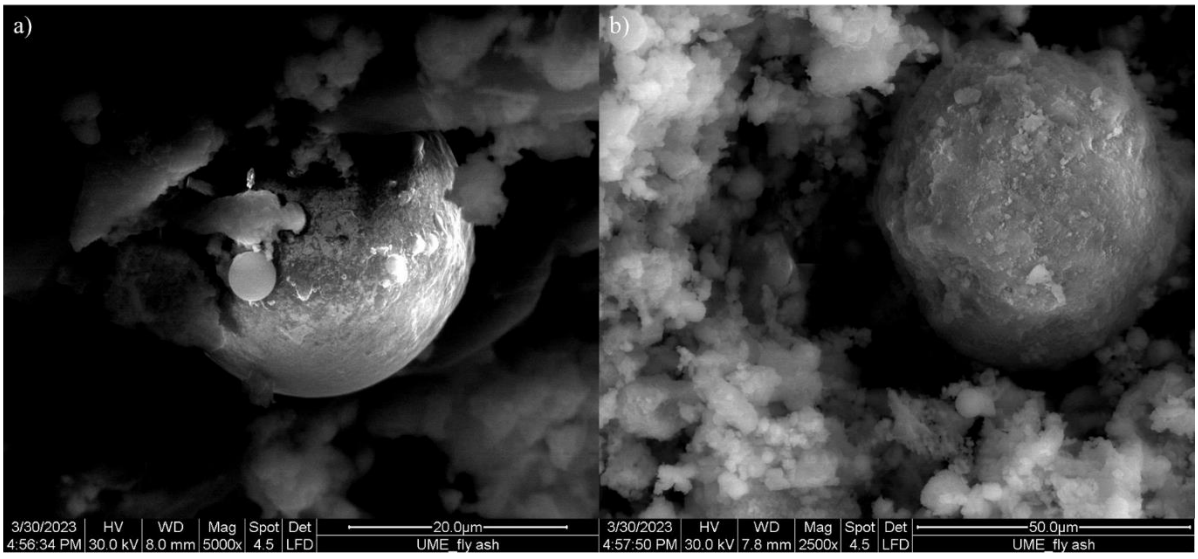

Figure 16: FA SEM images at a) 5000x and b) 2500x.

Figure 17 and Figure 18 display the SEM images of GPs 10 and 11, respectively. Both GPs have the same Si/Al ratio of 1.5. Notably, the two structures exhibit similarities, revealing a heterogeneous nature with a noticeable presence of unreacted precursor material.

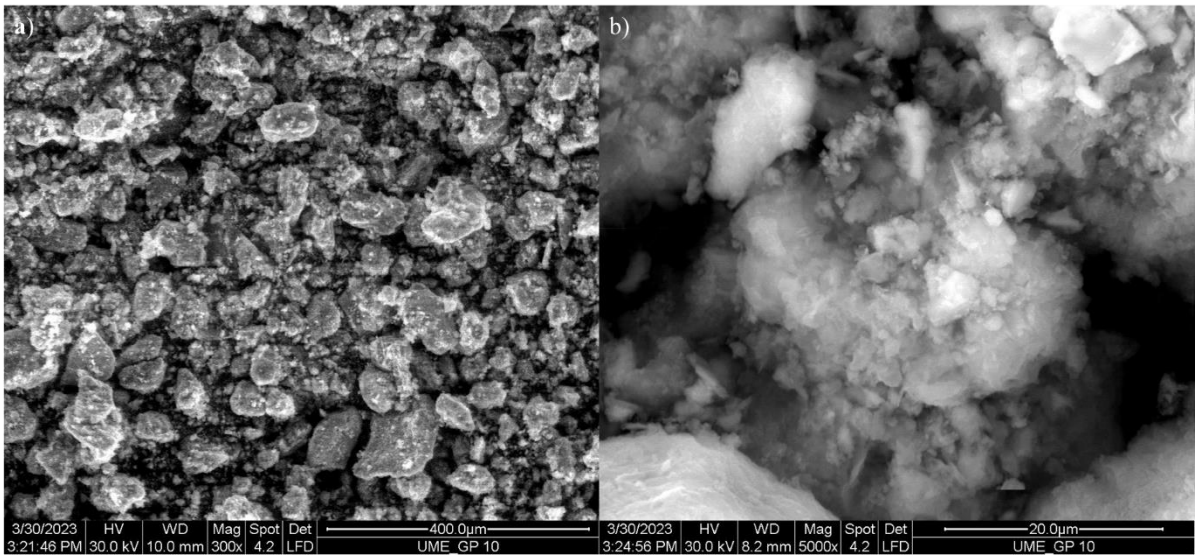

Figure 17: GP-10 SEM images at a) 300x and b) 5000x.

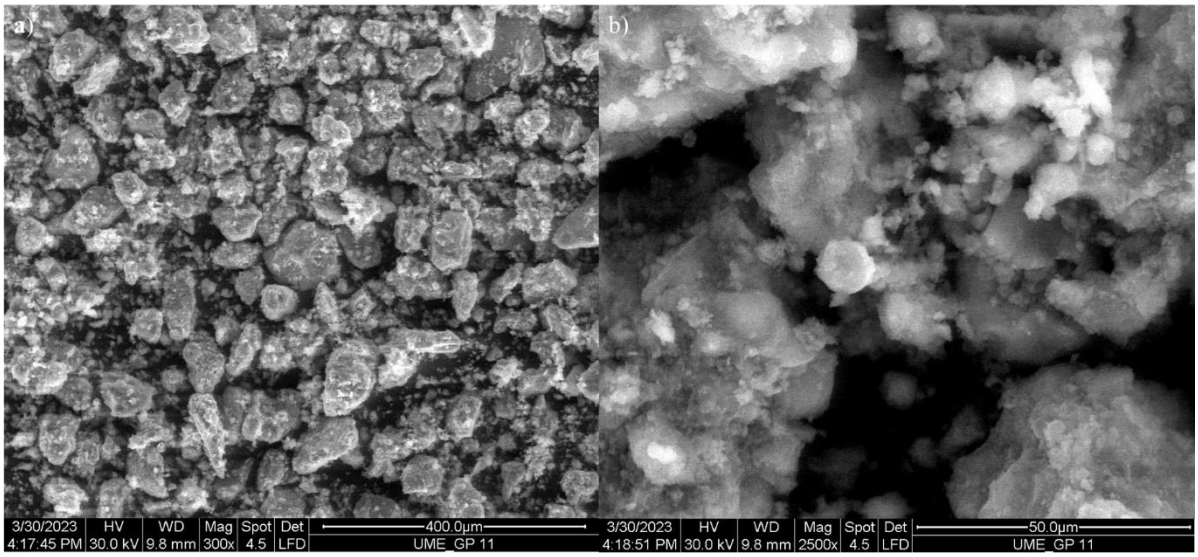

Figure 18: GP-11 SEM images at a) 300x and b) 2500x.

Figure 19 and Figure 20 display the SEM analysis of GPs 2 and 6, respectively. These two materials share the same Si/Al ratio of 2. These figures also demonstrate similarities in their structure, showing a heterogeneous appearance, unreacted FA particles, and relatively larger formed structures compared to Figure 16 and Figure 17.

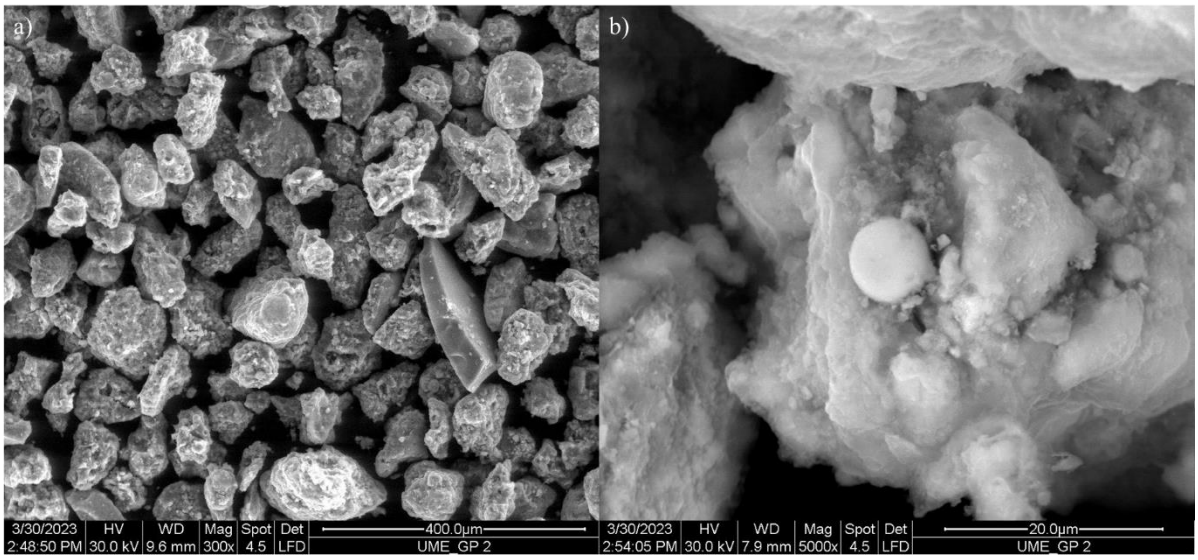

Figure 19: GP-2 SEM images at a) 300x and b) 5000x.

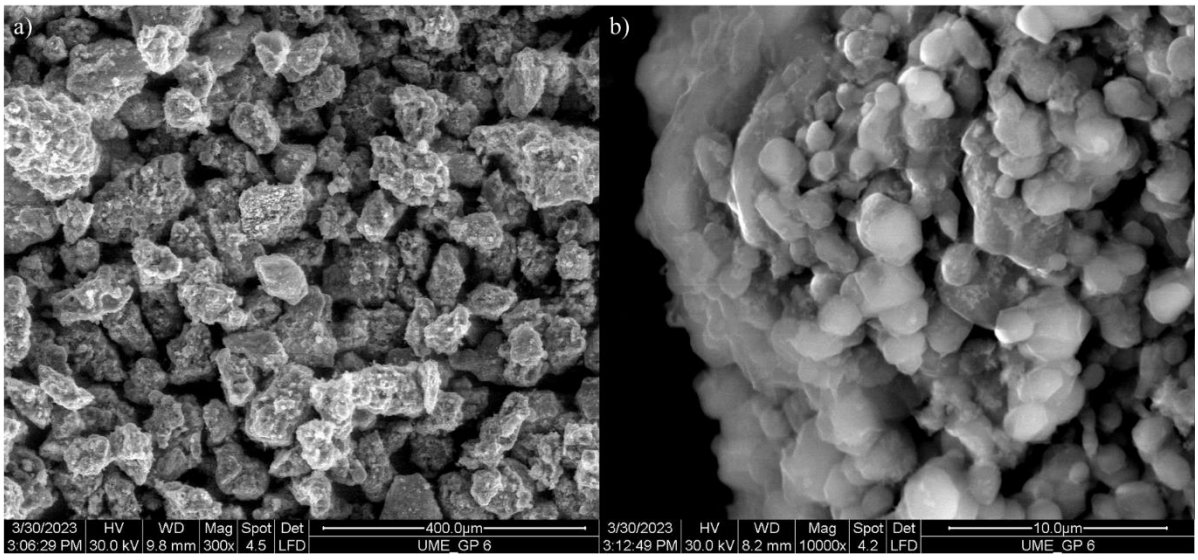

Figure 20: GP-6 SEM images at a) 300x and b) 10000x.

Figure 21 presents the SEM images of GP-13, which has a Si/Al ratio of 2.5. In contrast to the other analyzed GPs, GP-13 exhibits a more homogeneous structure with fewer unreacted FA particles.

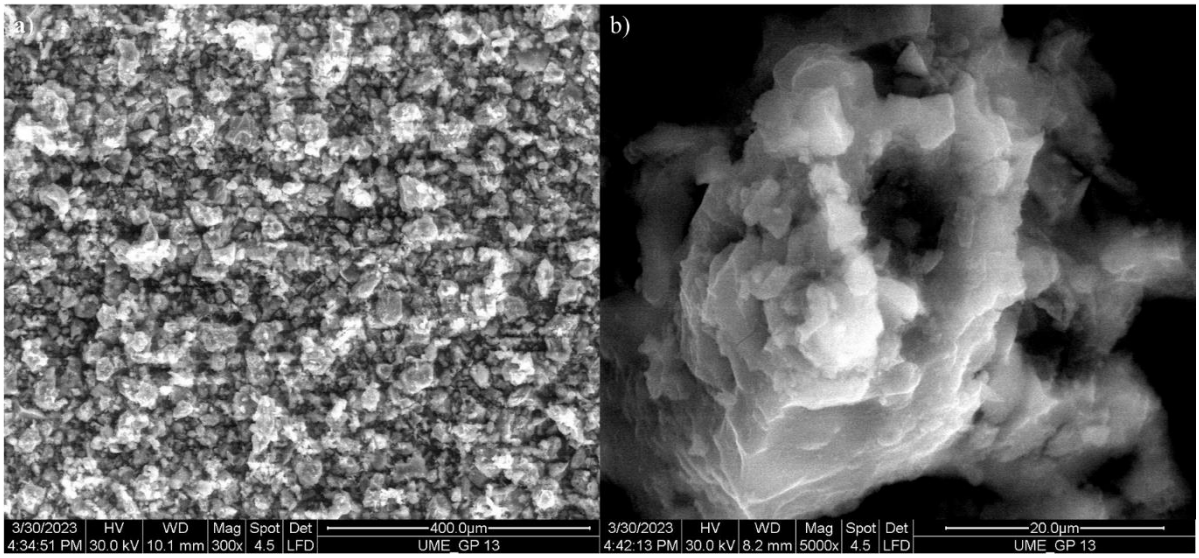

Figure 21: GP-13 SEM images at a) 300x and b) 5000x.

This analysis is consistent with a previous study that observed a correlation between Si/Al ratios and the structure of GPs. Lower Si/Al ratios tend to result in a less dense and unreacted structure, while higher Si/Al ratios lead to a denser and more homogeneous structure[148].

Furthermore, in Figure 21, it is possible to see how the pore size of GP-13 differs from the other GPs, confirming the results in Table 11. It is evident that GP-13 has larger pores compared to the other GPs, as indicated by the previous results. SEM images and analysis of the textural properties suggest a possible reason why GP-13 shows higher removal efficiency than other adsorbents. The larger surface area, volume, and pore size of GP-13 possibly facilitated the adsorption of gallic acid by providing more active sites for interaction.

SEM images also reveal that the geopolymerization product differs significantly from the spherical morphology of raw FA particles. Although a proportion of the FA particles remain undissolved, geopolymer formation is evident by its overlap with the surface of the FA particles[149].

The geopolymerization process results in the transformation of the surface material, rendering it more gel-like and porous. This change can be attributed to the alkaline activation process, which transforms the FA spherical particles into a geopolymer with an amorphous and porous structure[149]. Textural properties analysis (Table 11) confirms the increase in the GPs' porosity compared to the raw material. Additionally, the greater surface area of the geopolymer suggests that it is more effective as an adsorbent than FA[150].

The synthesized GPs exhibit an amorphous structure, meaning they have a random arrangement of molecules. This characteristic benefits adsorbent materials by providing large active sites, which can enhance adsorption. The amorphous structure of GPs allows for increased accessibility and availability of active sites, contributing to their effectiveness as adsorbents[151].

At last, in all microstructural images, it is possible to notice the microspheres present in the GPs; some studies suggest that the microspheres proffer the GPs outstanding characteristics, such as much better performance in strength and thermal insulation properties and low density[152–154].

5.2.5 X-RAY DIFFRACTION (XRD)

X-ray diffraction analysis was conducted to investigate the various phases in FA and GPs samples (GP-2, GP-6, GP-10, GP-11, GP-13). The resulting diffraction diagrams are presented in Figure 22.

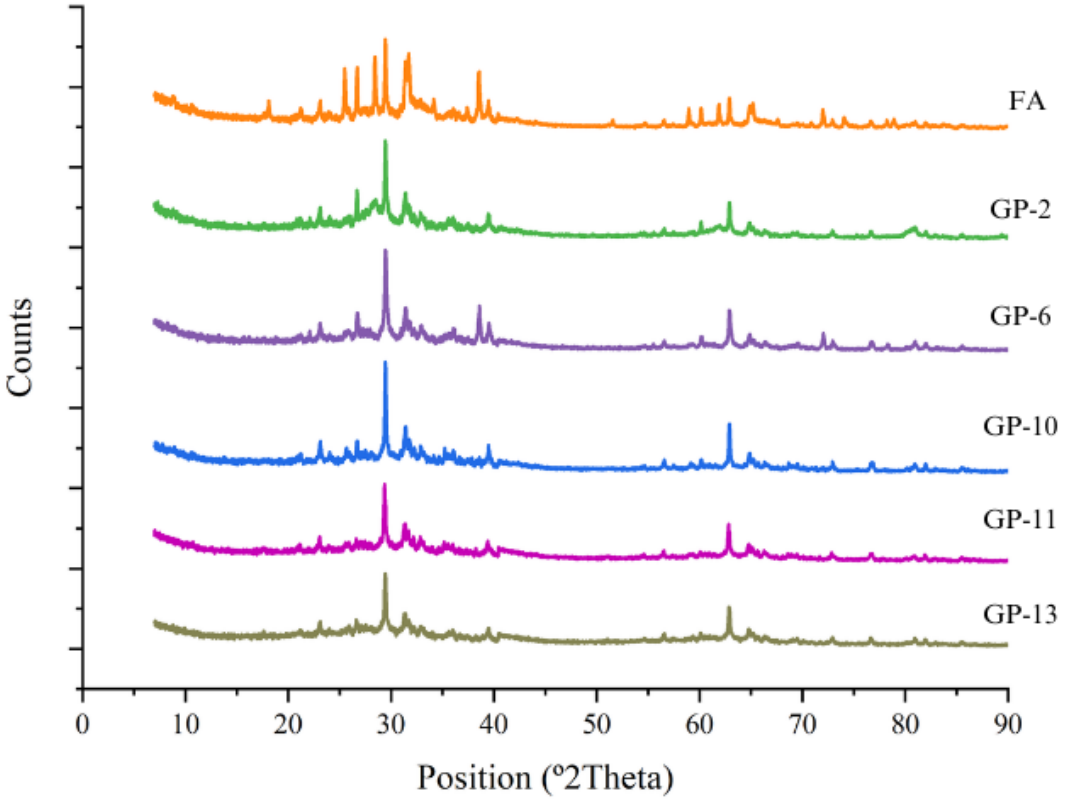

Figure 22: XRD patterns.

The X-ray diffraction (XRD) analysis of the FA revealed the presence of several crystalline phases, with calcite ($CaCO_3$) being the most prominent phase observed. This agrees with the ICP results (Table 10), which show that calcium is the most abundant element in FA.

Calcite, the predominant crystalline phase in geopolymeric materials, comprises calcium carbonate. Calcium carbonate is widely studied as an adsorbent due to its remarkable ability to remove heavy metals[155] and dyes[156]. These materials have gained attention in water treatment applications due to their affordability, ecology, and high surface area of their particles. Calcium carbonate's low cost and availability and efficient adsorption properties make it an attractive option for adsorbent in wastewater treatment[157].

The X-ray diffraction analysis also indicates that the main crystalline phase in FA are also present in the resulting GPs. This suggests the existence of undissolved FA particles in the final geopolymeric materials. Nevertheless, there is an increase in the intensity of the bands characteristic of amorphous phases, indicating that the aluminosilicate precursors undergo a reorganization process upon adding the alkali solution to form the geopolymer[158,159].

The presence of residual precursor particles in the geopolymer matrix offers opportunities to reuse or transform these materials into alternative forms. One innovative approach to reusing waste GPs is incorporating them into different geopolymer formulations. By reusing these GPs, the consumption of raw materials can be reduced, creating economic and environmental benefits. Recycling waste materials and using them as aluminosilicate sources shows promising prospects as it promotes greener production practices and contributes to global sustainable development. A notable example of this approach is demonstrated in the study conducted by Gharzouni et al.[155] investigating the mechanical properties of new GPs produced using waste geopolymer as a component.

Additionally, the broad peak detected between 2θ = 18º and 30º in the XRD pattern of FA, which is assigned to the amorphous phase of FA, is slightly displaced to higher angles (2θ = 21º - 35º) in the XRD patterns of the GPs. This implies that the amorphous FA phase is dissolved, and a new amorphous phase is formed during the synthesis of these materials[158,159].

5.2.6 ACID-BASE CHARACTERIZATION

The surface charge of GPs depends on the surrounding environment's pH. The surface may be positively charged, negatively charged, or have no charge at specific pH values. The pH at which the net charge on the particle is zero is referred to as the point of zero charge. This parameter is considered a significant descriptor of variable-charge surfaces. The results of pH_{PZC}, the values of pH during the adsorption tests (pH_{ads}), basicity, and acidity are shown in Table 12.

Table 12: Values of pH_{PZC}, pH_{ads}, basicity and acidity.

GP	pH_{PZC}	pH_{ads}	Basicity (mmol/L)	Acidity (mmol/L)
GP-2	8.18	7.82	12.3	1.00
GP-6	8.78	7.90	15.3	0.750
GP-10	8.66	8.10	13.0	0.300
GP-11	8.57	8.05	9.80	0.550
GP-13	8.23	7.97	10.5	1.40

The pH_{PZC} value for all the GPs analyzed was found to be in the range of 8. This suggests that the GPs will exhibit a positive charge below this value due to increased hydrogen ion (H+)

concentration. Conversely, when the pH exceeds this value, the GPs will carry a negative charge as hydroxide ions (OH−) concentration increases. The pH_{PZC} value is an essential parameter for describing variable-charge surfaces, and the consistency of values observed across the analyzed GPs indicates a uniform surface charge behavior[160].

As shown in Table 12, the pH values during the adsorption process for all GPs were lower than their pH_{PZC} values, indicating that the adsorbents were positively charged. On the other hand, gallic acid (GA) has four pK_a values (4.16, 8.55, 11.4, and 12.8)[161], which means that GA carries a negative charge at pH values above 4.16. Therefore, the adsorption of GA onto the tested GPs can be attributed to attractive electrostatic interactions between GP and GA molecules at this pH[162].

Some FA-derived geopolymer materials exhibited positive surface charges, effectively adsorbing negatively charged pollutants. One example is the geopolymer investigated by Siyal et al.[142] who examined the adsorption behavior of anionic surfactants. Considering this property of geopolymeric materials, it becomes plausible to investigate the adsorption potential of other negatively charged pollutants such as nitrate, nitrite, chloride, sulfide, and fluoride. Exploring the adsorption capacities of these geopolymeric materials for a broader range of contaminants would provide valuable information on their applicability as versatile adsorbents in water treatment applications.

Furthermore, under alkaline conditions, where the GPs acquire a negative surface charge, these geopolymeric materials have also demonstrated efficacy in removing positively charged pollutants. This versatility is exemplified by studies conducted by Darmayanti et al.[163], who investigated the adsorption of Cu^{2+} using geopolymer materials derived from FA, as well as by Li et al.[140], who examined the removal of dyes using GPs obtained from the same precursor. These findings highlight the broad applicability and adaptability of the geopolymeric material synthesized in this study, making it a promising candidate for diverse pollutant removal applications.

In Table 12, it can be seen that all of the analyzed GPs exhibit a predominantly basic character. Additionally, it can be observed that as the acidity of the GPs increases, the pH_{PZC} values decrease, which is a common trend observed for variable-charge surfaces.

5.3 GALLIC ACID ADSORPTION

5.3.1 KINETIC MODELLING

The influence of the processing time on the adsorption capacity of the adsorbent (in mg/g) was evaluated by investigating the adsorption kinetics. The kinetic models represented by Equations 4, 5, and 6 were fitted to experimental data of the adsorption kinetics. Table 13 presents the kinetic fitting data obtained for the adsorption of gallic acid onto the 15 different geopolymer samples.

Table 13: Parameters of kinetic models.

GP	q_{exp} (mg/g)	Pseudo-first-order			Pseudo-second-order			Intraparticle diffusion		
		q_e (mg/g)	k_1 (min^{-1})	R_1^2	q_e (mg/g)	k_2 (g/mg.min)	R_2^2	I (mg/g)	k_{id} ($mg/g.min_{0.5}$)	R_3^2
1	17.069	17.095	0.011	0.998	20.908	0.001	0.993	0.128	0.895	0.972
2	17.388	17.473	0.026	0.995	19.404	0.002	0.976	0.675	0.986	0.895
3	17.237	17.273	0.129	1.000	17.556	0.025	0.995	1.582	1.005	0.731
4	17.467	17.202	0.207	0.993	17.475	0.047	0.996	1.614	1.015	0.729
5	18.272	18.333	0.035	0.999	19.873	0.003	0.983	0.942	1.048	0.864
6	17.560	17.551	0.181	1.000	17.700	0.056	0.999	1.676	1.024	0.718
7	17.288	17.207	0.085	1.000	17.827	0.010	0.993	1.399	1.005	0.773
8	17.276	17.499	0.030	0.976	19.140	0.002	0.951	0.804	0.991	0.868
9	17.731	17.710	0.381	1.000	17.717	1.241	1.000	1.750	1.032	0.704
10	17.153	16.945	0.232	0.998	17.113	0.078	0.999	1.617	0.997	0.722
11	17.281	17.268	0.239	1.000	17.343	0.129	1.000	1.681	1.008	0.711
12	17.393	17.421	0.036	0.987	18.901	0.003	0.958	0.912	0.997	0.850
13	18.037	17.755	0.150	0.997	18.090	0.028	1.000	1.624	1.044	0.738
14	17.627	17.530	0.082	0.999	18.194	0.010	0.996	1.407	1.024	0.777
15	17.869	17.942	0.057	0.987	18.935	0.005	0.961	1.257	1.036	0.799

Observing the value of R^2, the obtained results indicate that, in general, the pseudo-first-order model fit better with experimental data. Additionally, the calculated adsorptive capacity in the equilibrium (q_e) for these GPs and this model was closer to the experimental data (q_{exp}), validating its applicability in the description of gallic acid adsorption kinetics data.

Other studies investigating adsorption onto adsorbent GPs have reported similar results to those obtained in this study. Alouani et al.[164] studied the adsorption of Rhodamine B dye and obtained better fits with the pseudo-first-order kinetic model. Similarly, Rocha et al.[165] found a

higher R^2 value for the pseudo-first-order kinetic model in their investigation of copper removal.

GPs 4, 10, and 13 showed the R^2 value slightly more prominent for the pseudo-second-order model and the experimental adsorptive capacity (q_{exp}) value closest to the value calculated (q_e) by the pseudo-second-order model. Interestingly, GPs 9 and 11 exhibited R^2 values of 1 for both the pseudo-first order and pseudo-second-order models, indicating a good fit for the two models.

For the GPs that best fit the pseudo-second-order model, comparable results were found in the literature that also produced GPs from FA. Purbasari et al.[166] observed the best fit of the pseudo-second-order model for removing Cu(II) and Fe(II). Zhang and Liu[164] studied dye adsorption and obtained a better fit with the pseudo-second-order model. Liu et al.[167] found that the same model provided the best fit for Pb removal.

This study investigated the adsorption rate regarding possible limiting steps of liquid film diffusion, intraparticle diffusion, or both. Analysis of the intraparticle diffusion model fit revealed that the R^2 values were all below 0.980 for the GPs examined, and the intercept (I) was not equal to zero, suggesting that intraparticle diffusion was probably not the only rate-limiting step. Hence, it can be inferred that the kinetics of the adsorption process was probably controlled by both the liquid film and intraparticle diffusion[168].

Furthermore, Figure 23 illustrates the graphs describing the fits of the three kinetic models relative to the experimental data evaluated for GPs 2, 6, 10, 11, and 13.

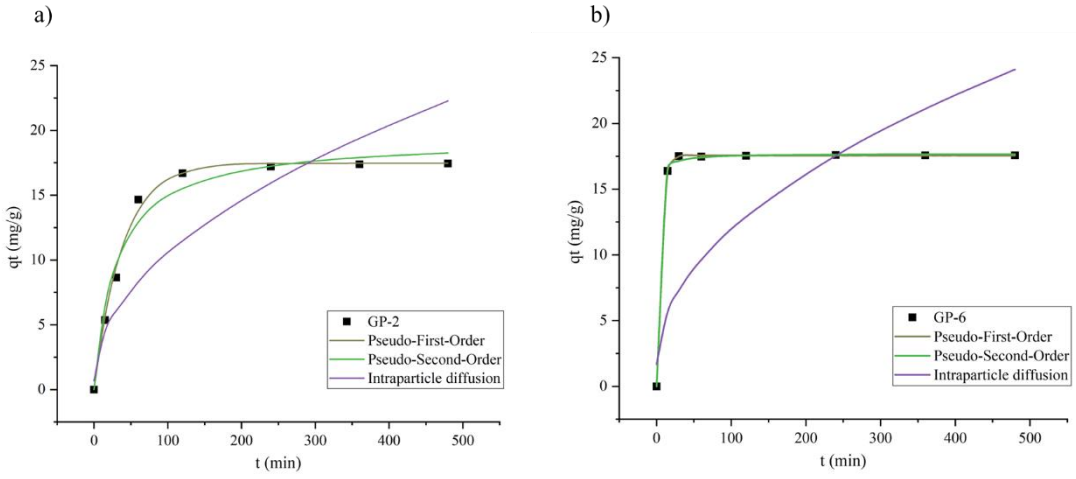

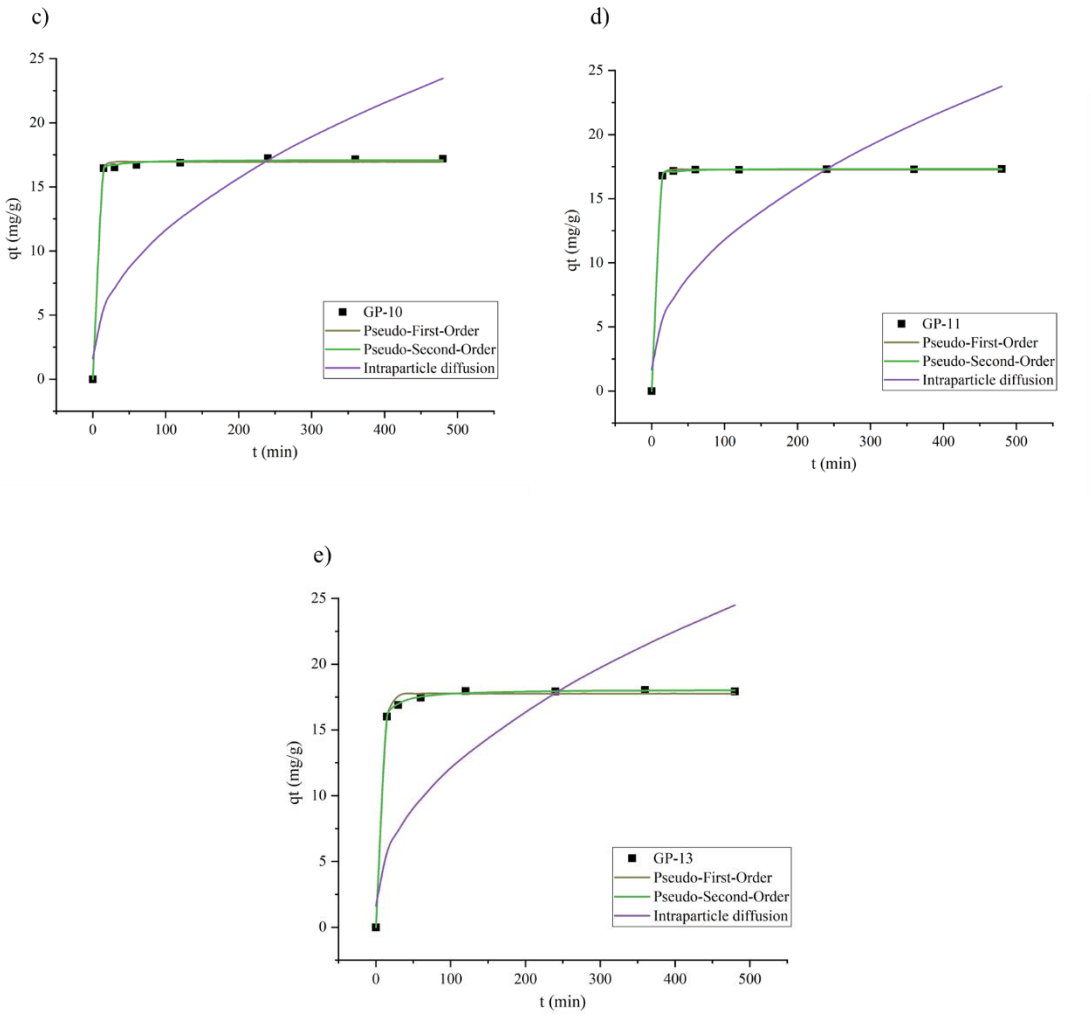

Figure 23: Fitting the kinetic models to the experimental data for a) GP-2; b) GP-6; c) GP-10; d) GP-11 and e) GP-13.

The plotted graphs provide a more transparent visual representation of how the three kinetic models fit the experimental data. For all materials, during the initial stages of adsorption, there is an increase in the amount of gallic acid retained per unit mass of adsorbent. This occurs because, during this period, active sites have greater availability, favoring higher adsorption rates. As time passes, the number of active sites available to adsorb the GA decreases, and the already adsorbed pollutant molecules prevent the entry of new molecules. As a result, the kinetics slows until equilibrium is reached, where no significant variations in adsorption capacity are observed over time.

During the initial minutes of the adsorption process, there is a rapid and significant increase in adsorbate retention, followed by equilibrium at approximately 200 minutes. Geopolymer 2 presents a slightly different behavior, the increase in the response variable is not

as fast in the beginning when compared with the other GPs and its equilibrium is reached around 300 minutes. Moreover, it is noticeable that GPs 6, 10, 11, and 13 exhibit similar behavior.

5.3.2 EQUILIBRIUM ISOTHERMS

The equilibrium isotherms were studied by fitting the Langmuir and Freundlich's models described by Equations 7 and 9, respectively to the experimental data. Table 14 shows the parameters obtained by the equilibrium fits for GPs 2, 6, 10, 11, and 13.

Table 14: Parameters of equilibrium models.

GP	Langmuir			Freundlich		
	q_{max} (mg/g)	K_L (L/mg)	R^2	K_F (L/g)	n_F	R^2
2	39.241	0.422	0.982	11.439	2.197	0.988
6	75.839	0.445	0.989	22.017	1.401	0.972
10	58.115	0.215	0.980	10.616	1.605	0.982
11	41.651	0.781	0.956	15.713	1.989	0.958
13	40.837	1.810	0.958	21.999	2.366	0.965

Analyzing the values of R^2 obtained in the adjustments of each of the models for the GPs, it can be observed that both models adequately described the experimental data of equilibrium. The highest R^2 values were obtained in the Freundlich model except for geopolymer 6, which showed this higher value for the Langmuir model.

The findings obtained in this study can be compared to previous research that utilized fly ash (FA) to produce geopolymer-based adsorbents. Duan et al.[169] investigated the removal of Cu(II) from wastewater and observed a satisfactory fit for the Freundlich and Langmuir models. Tian and Sasaki[170] found a better fit for the Freundlich model when they studied the adsorption of arsenate (AsO_4^{3-}). And also, Qiu et al.[171] reported a better fit of the Freundlich model in removing Cr(VI).

For GP-6 that obtained a better fit to the Langmuir model, other studies have also found the same result for GPs produced from the same precursor. Liu et al.[167] reported a better fit in their equilibrium data on Pb removal with the Langmuir model, just as Purbasari et al.[172] showed a better fit with the same model in studying the removal of anionic and cationic dyes.

The best fit of the isotherms to the Freundlich model proposes that adsorption occurs on solids with heterogeneous surfaces, where the active sites have varying affinities and adsorption energies. Sites with the highest affinity for the adsorbed molecules will be preferentially occupied. This results in a decrease in the binding energy of the remaining sites, following an exponential decay profile. Then the multilayer arrangement is formed during the adsorption process[173]. However, it is impossible to state that GPs exhibit this behavior during adsorption since the Langmuir model was also well-fitted to the experimental data, and further studies are needed for more profound conclusions.

By further analyzing the obtained n_F values from fitting the Freundlich model, it is evident that all the values fall within the expected range of 1 to 10, indicating favorable conditions for adsorption. Furthermore, by examining the calculated R_L values using Equation 8 (Table 15), it can be seen that all values are between 0 and 1. This indicates a meaningful affinity of the adsorbate for the adsorbent, which suggests good adsorption processes for all the GPs analyzed.

Table 15: R_L calculated values.

C_0 (mg/L)	**R_L**				
	Geopolymer Sample				
	2	**6**	**10**	**11**	**13**
100	0.02	0.02	0.04	0.01	0.01
75	0.03	0.03	0.06	0.02	0.01
50	0.05	0.04	0.09	0.02	0.01
30	0.07	0.07	0.13	0.04	0.02
10	0.19	0.18	0.32	0.11	0.05

Figure 24 displays the plots describing the fits of the two equilibrium models for the five geopolymer samples. These graphs visually represent how the models fit with the experimental data.

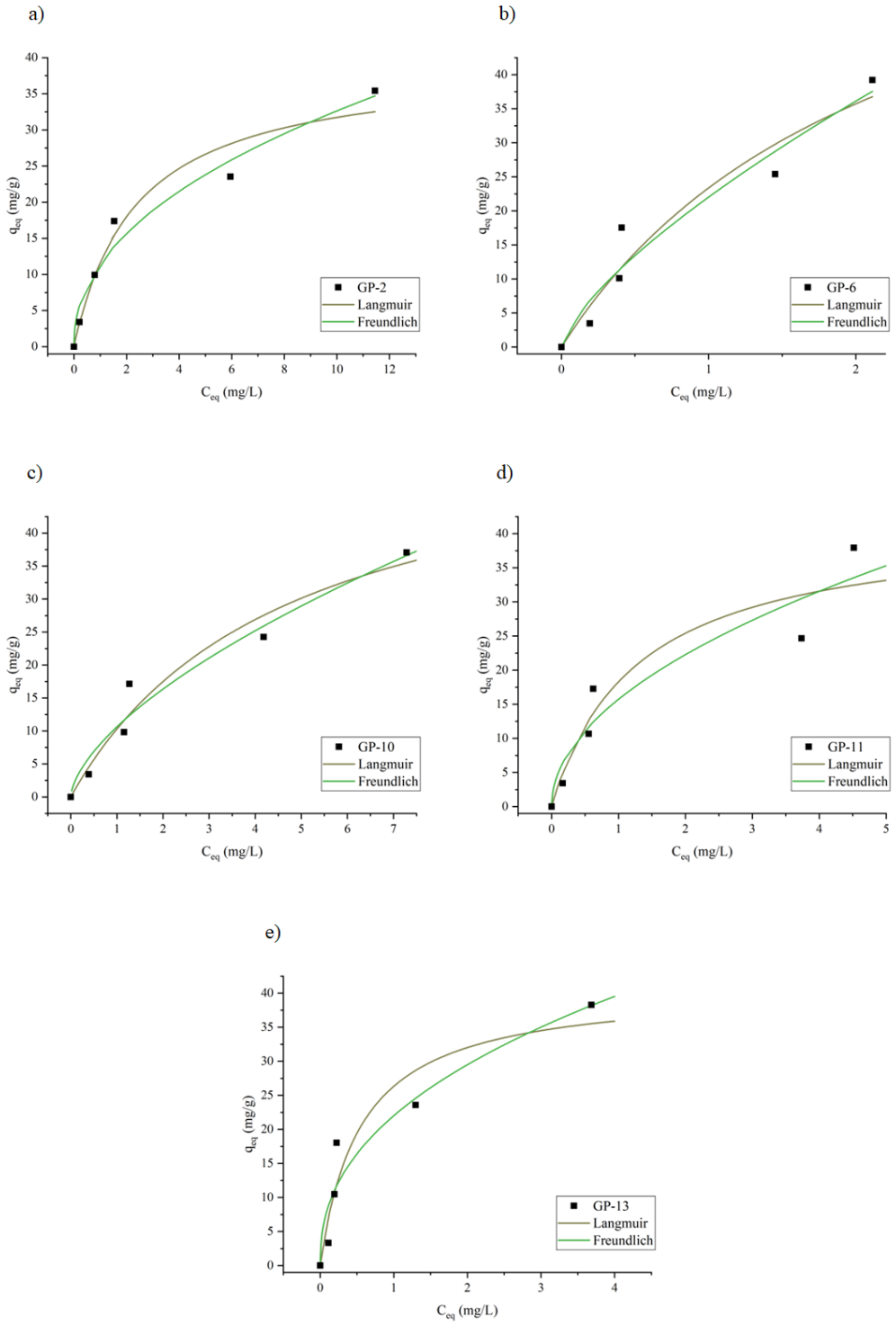

Figure 24: Adsorption isotherms using Langmuir and Freundlich for a) GP-2; b) GP-6; c) GP-10; d) GP-11 and e) GP-13.

The results of the Langmuir fit show that the highest adsorption capacities were obtained by GP-6 and GP-10, with values of 75.8 mg/g and 58.1 mg/g, respectively. The other GPs

exhibited similar adsorption capacities around 40 mg/g. Notably, the GPs with a higher molar concentration of NaOH (10 M) showed the highest adsorption capacities. Additionally, GP-6 stands out as the only geopolymer with the maximum ratio of Na_2SiO_3/NaOH in its formulation, which may have also contributed to its superior adsorptive capacity.

6 CONCLUSIONS AND FUTURE RESEARCH

6.1 CONCLUSIONS

Developing geopolymeric adsorbent materials using FA as a precursor for removing GA, representing a basic compound of phenolic compounds found in model wastewater, was possible. All the produced GPs played a satisfactory role as adsorbents and were able to remove the target pollutant.

Using a BBD with three main factors, namely, the Si/Al mass ratio, the NaOH molar concentration, and the Na_2SiO_3/NaOH mass ratio, was a useful tool for the production of the GPs. The contour plots and statistical data analysis revealed that the Si/Al ratio had the highest statistical significance, as indicated by its p-value << 0.05, concerning the evaluated response, which GA removal (%).

Moreover, some GPs produced and the FA were characterized. The ICP-OES analysis of the FA revealed its composition, predominantly consisting of calcium, silica, and aluminum, establishing its suitability as an excellent source of aluminosilicates for GP synthesis. Porosimetry and surface area analysis demonstrated significant improvements in the GPs compared to the FA, evident from the enhanced BET surface area (m^2/g), total pore volume (cm^3/g), and average pore size (nm). Notably, GP-13 exhibited a remarkable surface area of 61 m^2/g. FT-IR analysis confirmed the occurrence of geopolymerization through the presence of characteristic peaks indicating the presence of H_2O, carbonate ions, and silicon, oxygen, and aluminum bonds.

The SEM analysis revealed structural differences between the GPs with varying Si/Al ratios, along with the identification of unreacted FA particles in the structures of the GPs. XRD analysis revealed the predominance of calcite as the crystalline phase in both FA and GPs, and confirmed the amorphous nature of the materials produced. Furthermore, acid-base characterization demonstrated the predominantly basic nature of the GPs, and the resulting pHpzc values were generally around 8, indicating their positive charge during the adsorption process. The electrostatic attraction observed between the positively charged GPs and gallic acid probably played a significant part in the facilitation of the adsorption phenomena.

The adsorption kinetics tests performed on the GPs exhibited a flattering fit to the pseudo-first-order model. Also, they showed that during the initial stages of adsorption, there was a

rapid increase in the amount of GA adsorbed per unit mass of adsorbent until reaching equilibrium in approximately 200 minutes. The equilibrium study additionally revealed that the GPs generally fit the Freundlich model better. Notably, the calculated n_F values indicated favorable conditions for adsorption, while the R_L values indicated significant affinity between the adsorbate and the adsorbent. Among the analyzed GPs, GP-6 showed the highest maximum adsorption capacity (q_{max}) value, reaching 75.839 mg/g.

This study demonstrated the significant potential of using waste precursors to produce materials with added value, aligning with the principles of the CE. By reintegrating waste into the economic cycle, positive impacts are seen on all three pillars of sustainable development: society, economy, and environment. The materials developed not only contribute to waste reduction by shifting waste away from storage or landfill, but also demonstrate effective removal of pollutants from wastewater. These findings highlight the importance of finding innovative and sustainable solutions in materials development, promoting a more resource-efficient and environmentally conscious future.

6.2 FUTURE RESEARCH

This study developed GPs from waste material, FA, and investigated their adsorption potential of gallic acid as a standard compound for phenolic content. Future research directions could explore the application of these GPs into real wastewater, such as leached, closing the loop of the circular economy.

In the adsorption of other pollutants such as heavy metals, surfactants and dyes to assess their performance in a broader range of contaminants. Moreover, investigating desorption techniques to recover the adsorbate for potential reuse in other applications would be interesting.

Evaluating GPs in different formats, such as membranes or spheres, could provide insights into their adsorption performance and incorporate other components into the matrix of GPs to improve their performance, such as activated carbons and catalysts and carbon nanotubes.

Exploring alternative waste materials as precursors, such as residual diatomaceous earth, red mud, and slag, for synthesizing GPs and evaluating their adsorption capacity and efficiency

in water treatment may contribute to expanding the range of possible precursors for developing GPs.

Additionally, further investigations can explore other factors influencing adsorption that were not considered in this study, such as temperature variation, pH, agitation, and adsorbent dosage.

REFERENCES

1. Chand Malav L, et al. A review on municipal solid waste as a renewable source for waste-to-energy project in India: Current practices, challenges, and future opportunities. *J Clean Prod*. 2020;277:123227. doi:10.1016/J.JCLEPRO.2020.123227
2. Trends in Solid Waste Management. Accessed July 14, 2022. https://datatopics.worldbank.org/what-a-waste/trends_in_solid_waste_management.html
3. Song Q, Li J, Zeng X. Minimizing the increasing solid waste through zero waste strategy. *Journal of Cleaner Production*. Published online 2014. doi:10.1016/j.jclepro.2014.08.027
4. Circular economy action plan. Accessed July 14, 2022. https://environment.ec.europa.eu/strategy/circular-economy-action-plan_pt
5. A new Circular Economy Action Plan. Accessed July 14, 2022. https://eur-lex.europa.eu/legal-content/EN/TXT/?qid=1583933814386&uri=COM:2020:98:FIN
6. Novais R et al. Waste glass from end-of-life fluorescent lamps as raw material in geopolymers. *Waste Management*. 2016;52:245-255. doi:10.1016/j.wasman.2016.04.003
7. Nanda S, Berruti F. A technical review of bioenergy and resource recovery from municipal solid waste. *Journal of Hazardous Materials*. 2021;403. doi:10.1016/j.jhazmat.2020.123970
8. Ren B et al. Eco-friendly geopolymer prepared from solid wastes: A critical review. *Chemosphere*. 2021;267. doi.org:10.1016/j.chemosphere.2020.128900
9. Singh N, Middendor B. Geopolymers as an alternative to Portland cement: An overview. *Construction and Building Materials*. 2020;237. doi:10.1016/j.conbuildmat.2019.117455
10. Glasby T, et al. EFC Geopolymer Concrete Aircraft Pavements at Brisbane West Wellcamp Airport. 2015:1-9.
11. Davidovits J. Geopolymers: man-made rock geosynthesis and the resulting development of very early high strength cement. *Materials Education*. 1994;16:91-139.
12. Davidovits J. 30 years of successes and failures in geopolymer applications. Market trends and potential breakthroughs. *Geopolymer 2002 conference*. 2002:28-29. Accessed July 14, 2022. https://www.geopolymer.org/wp-content/uploads/30YearsGEOP.pdf

13. Al-Ghouti MA et al. Application of geopolymers synthesized from incinerated municipal solid waste ashes for the removal of cationic dye from water. *PLoS One*. 2020;15(11). doi:10.1371/JOURNAL.PONE.0239095

14. Maleki A et al. Adsorbent materials based on a geopolymer paste for dye removal from aqueous solutions. *Arabian Journal of Chemistry*. 2020;13:3017-3025. doi:10.1016/j.arabjc.2018.08.011

15. Tan T et al. Synthesis of porous geopolymer sphere for Ni (II) removal. *Ceramics International*. 2021;47:29055-29063. doi: 10.1016/j.ceramint.2021.06.268

16. Siyal A et al. Optimization of synthesis of geopolymer adsorbent for the effective removal of anionic surfactant from aqueous solution. *Journal of Environmental Chemical Engineering*. 2021;9. doi:10.1016/j.jece.2020.104949

17. DIRECTIVE 2008/98/EC OF THE EUROPEAN PARLIAMENT AND OF THE COUNCIL of 19 November 2008 on waste and repealing certain Directives (Text with EEA relevance).

18. Wastes | US EPA. Accessed July 14, 2022. https://www.epa.gov/report-environment/wastes#note1

19. Waste statistics - Statistics Explained. Accessed July 15, 2022. https://ec.europa.eu/eurostat/statistics-explained/index.php?title=Waste_statistics#Waste_generation_excluding_major_mineral_waste

20. Kanhai G et al. Urban Municipal Solid Waste management: Modeling air pollution scenarios and health impacts in the case of Accra, Ghana. *Waste Management*. 2021;123:15-22. doi:10.1016/j.wasman.2021.01.005

21. Bekchanov M, Mirzabae A. Circular economy of composting in Sri Lanka: Opportunities and challenges for reducing waste related pollution and improving soil health. *Journal of Cleaner Production*. 2018;202:1107-1119. doi:10.1016/j.jclepro.2018.08.186

22. Ighalo J et al. A systematic literature analysis of the nature and regional distribution of water pollution sources in Nigeria. *Journal of Cleaner Production*. 2021;283. doi: 10.1016/j.jclepro.2020.124566.

23. Blair J, Mataraarachchi S. A Review of Landfills, Waste and the Nearly Forgotten Nexus with Climate Change. *Environments*. 2021;8. doi:10.3390/environments8080073

24. Law KL et al. The United States' contribution of plastic waste to land and ocean. *Sci Adv*. 2020;6(44). doi:10.1126/SCIADV.ABD0288

25. Shah A et al. Municipal solid waste as a sustainable resource for energy production: State-of-the-art review. *Journal of Environmental Chemical Engineering*. 2021;9. doi:10.1016/j.wasman.2016.04.003

26. EU-27: municipal waste generation 2004-2020 | Statista. Accessed October 6, 2022. https://www.statista.com/statistics/983592/municipal-waste-generation-european-union-eu-28/

27. Municipal waste, Generation and Treatment. Accessed July 14, 2022. https://stats.oecd.org/Index.aspx?DataSetCode=MUNW#

28. Speight JG. Waste gasification for synthetic liquid fuel production. *Gasification for Synthetic Fuel Production*. 2015:277-301. doi:10.1016/B978-0-85709-802-3.00012-6

29. Wilson DC. International Solid Waste Association. *Global Waste Management Outlook*.

30. New World Bank country classifications by income level: 2021-2022. Accessed September 14, 2022. https://blogs.worldbank.org/opendata/new-world-bank-country-classifications-income-level-2021-2022

31. Adhikari S, Nam H, Chakraborty JP. Conversion of solid wastes to fuels and chemicals through pyrolysis. *Waste Biorefinery*. 2018:239-263. doi:10.1016/B978-0-444-63992-9.00008-2

32. Diaz-Barriga-Fernandez AD et al. Strategic Planning for Managing Municipal Solid Wastes with Consideration of Multiple Stakeholders. *ACS Sustain Chem Eng*. 2017;5(11):10744-10762. doi:10.1021/ACSSUSCHEMENG.7B02717/SUPPL_FILE/SC7B02717_SI_001.PDF

33. Cudjoe D, Acquah PM. Environmental impact analysis of municipal solid waste incineration in African countries. *Chemosphere*. 2021;265. doi:10.1016/j.chemosphere.2020.129186

34. He P et al. Municipal solid waste (MSW) landfill: A source of microplastics? -Evidence of microplastics in landfill leachate. *Water Res*. 2019;159:38-45. doi:10.1016/J.WATRES.2019.04.060

35. Ali IH et al. Contamination and human health risk assessment of heavy metals in soil of a municipal solid waste dumpsite in Khamees-Mushait, Saudi Arabia. *Toxin Rev*. 2021;40(1):102-115. doi:10.1080/15569543.2018.1564144

36. Samadi MT et al. Characteristics and health effects of potentially pathogenic bacterial aerosols from a municipal solid waste landfill site in Hamadan, Iran. *J Environ Health Sci Eng*. 2021;19(1):1057-1067. doi:10.1007/S40201-021-00672-3

37. Municipal waste statistics - Statistics Explained. Accessed July 14, 2022. https://ec.europa.eu/eurostat/statistics-explained/index.php?title=Municipal_waste_statistics&oldid=569515

38. Krook J, Svensson, Eklund M. Landfill mining: A critical review of two decades of research. *Waste Management*. 2012;32:513-520. doi:10.1016/j.wasman.2011.10.015

39. Luo H et al. Recent advances in municipal landfill leachate: A review focusing on its characteristics, treatment, and toxicity assessment. *Science of the Total Environment*. 2020;703. doi:10.1016/j.scitotenv.2019.135468

40. Mahtab M, Islam D, Farooqi IH. Optimization of the process variables for landfill leachate treatment using Fenton based advanced oxidation technique. *Engineering Science and Technology an International Journal*. 2021;24:428-435. doi:10.1016/j.jestch.2020.08.013

41. Kumar A, Samadder SR. A review on technological options of waste to energy for effective management of municipal solid waste. *Waste Management*. 2017;69:407-422. doi:10.1016/j.wasman.2017.08.046

42. Zhao Y et al. Environmental impact assessment of the incineration of municipal solid waste with auxiliary coal in China. *Waste Management*. 2012;32:1989-1998. doi:10.1016/j.wasman.2012.05.012

43. Li X et al. Utilization of municipal solid waste incineration bottom ash in blended cement. *Journal of Cleaner Production*. 2012;32:96-100. doi:10.1016/j.jclepro.2012.03.038

44. Training Package on EU Waste Legislation - Environment - European Commission. Accessed July 14, 2022. https://ec.europa.eu/environment/legal/law/6/module_1_3.htm

45. Knickmeyer D. Social factors influencing household waste separation: A literature review on good practices to improve the recycling performance of urban areas. *Journal of Cleaner Production*. 2020;245. doi:10.1016/j.jclepro.2019.118605

46. Lobo M, Dorta E. Utilization and management of horticultural waste. *Postharvest Technology of Perishable Horticultural Commodities*. 2019:639-666. doi:10.1016/B978-0-12-813276-0.00019-5

47. Petruccioli M et al. Agriculture and Agro-Industrial Wastes, Byproducts, and Wastewaters: Origin, Characteristics, and Potential in Bio-Based-Compounds Production. *Comprehensive Biotechnology, Second Edition*. 2011;6:531-545. doi:10.1016/B978-0-08-088504-9.00389-5

48. Suarez-Eiroa B et al. Operational principles of circular economy for sustainable development: Linking theory and practice. *Journal of Cleaner Production*. 2019;214:952-961. doi:10.1016/j.jclepro.2018.12.271

49. Grafström J, Aasma S. Breaking circular economy barriers. *J Clean Prod*. 2021;292:126002. doi:10.1016/J.JCLEPRO.2021.126002

50. Tsang Y et al. Production of bioplastic through food waste valorization. *Environment International*. 2019;127:625-644. doi:10.1016/j.envint.2019.03.076

51. Kapoor R et al. Valorization of agricultural waste for biogas based circular economy in India: A research outlook. *Bioresource Technology*. 2020;304. doi:10.1016/j.biortech.2020.123036

52. Su G et al. Valorisation of medical waste through pyrolysis for a cleaner environment: Progress and challenges. *Environmental Pollution*. 2021;279. doi:10.1016/j.envpol.2021.116934

53. Yatsenko EA et al. Eco-Geopolymers Based on CHP Plant Ash-Slag Waste: Promising Materials for Road Construction in the Arctic Zone. *Glass and Ceramics*. 2022;78(11-12):490-493. doi:10.1007/S10717-022-00438-9

54. Kabongo JD. Waste Valorization. In: Idowu Samuel O. and Capaldi N and ZL and GA das, ed. *Encyclopedia of Corporate Social Responsibility*. Springer Berlin Heidelberg; 2013:2701-2706. doi:10.1007/978-3-642-28036-8_680

55. Nzihou A, Lifset R. Waste Valorization, Loop-Closing, and Industrial Ecology. *J Ind Ecol*. 2010;14(2):196-199. doi:10.1111/j.1530-9290.2010.00242.xï

56. Ghumra DP, Rathi O, Mule TA, et al. Technologies for valorization of municipal solid wastes. *Biofuels, Bioproducts and Biorefining*. 2022;16(3):877-890. doi:10.1002/BBB.2340

57. Scarlat N, Dallemand JF, Fahl F. Biogas: Developments and perspectives in Europe. *Renew Energy*. 2018;129:457-472. doi:10.1016/J.RENENE.2018.03.006

58. Waste recycling in Europe. Accessed July 21, 2022. https://www.eea.europa.eu/ims/waste-recycling-in-europe

59. Landfill waste. Accessed July 22, 2022. https://environment.ec.europa.eu/topics/waste-and-recycling/landfill-waste_en

60. Zhuang X et al. Fly ash-based geopolymer: clean production, properties and applications. *Journal of Cleaner Production*. 2016;125:253-267. doi:10.1016/j.jclepro.2016.03.019

61. Ghassemi M et al. Hazardous Waste from Fossil Fuels. *Encyclopedia of Energy*. Published online 2004:119-131. doi:10.1016/B0-12-176480-X/00395-8

62. Ahmaruzzaman M. A review on the utilization of fly ash. *Prog Energy Combust Sci*. 2010;36(3):327-363. doi:10.1016/J.PECS.2009.11.003

63. Soni R, Bhardwaj S, Shukla DP. Various water-treatment technologies for inorganic contaminants: current status and future aspects. *Inorganic Pollutants in Water*. Published online January 1, 2020:273-295. doi:10.1016/B978-0-12-818965-8.00014-7

64. Ukwattage NL, Ranjith PG, Bouazza M. The use of coal combustion fly ash as a soil amendment in agricultural lands (with comments on its potential to improve food security and sequester carbon). *Fuel*. 2013;109:400-408. doi:10.1016/J.FUEL.2013.02.016

65. Kováèik P et al. Effect of ash-fly ash mixture application on soil fertility. *Journal of Elementology*. 2016;52:245-255. doi:10.5601/jelem.2011.16.2.05

66. Cetin S, Pehlivan E. The use of fly ash as a low cost, environmentally friendly alternative to activated carbon for the removal of heavy metals from aqueous solutions. *Colloids Surf A Physicochem Eng Asp*. 2007;298(1-2):83-87. doi:10.1016/J.COLSURFA.2006.12.017

67. Cheng H, Zhou Y, Liu Q. Kaolinite nanomaterials: preparation, properties and functional applications. *Nanomaterials from Clay Minerals*. 2019:285-334. doi:10.1016/B978-0-12-814533-3.00006-5

68. Alzeer M, MacKenzieb KJD. Fiber composites of inorganic polymers (geopolymers) reinforced with natural fibers. *Composite Materials*. 2021:117-147. doi:10.1016/B978-0-12-820512-9.00016-2

69. Ivanova E, Bazaka K, Crawford R. New functional biomaterials for medicine and healthcare. Published online 2014. Accessed July 14, 2022. https://www.cambridge.org/core/journals/mrs-bulletin/article/photonic-crystals-principles-and-applications-editors-qihuang-gong-and-xiaoyong-hu/34A485D0FFE7CF6136FC6F516D6B7A2A

70. Giacobello F et al. Geopolymers and Functionalization Strategies for the Development of Sustainable Materials in Construction Industry and Cultural Heritage Applications: A Review. *Materials (Basel)*. 2022;15. doi:10.3390/ma15051725

71. Siyal A et al. A review on geopolymers as emerging materials for the adsorption of heavy metals and dyes. *Journal of Environmental Management*. 2020;258. doi:10.1016/j.jclepro.2020.120896

72. Srinivasan K, Sivakumar A. Geopolymer binders: a need for future concrete construction. *International Scholarly Research Notices*. 2013;2013. doi:10.1155/2013/509185

73. Zhang P et al. Fabrication and engineering properties of concretes based on geopolymers/alkali-activated binders-A review. *Journal of Cleaner Production*. 2016;52:245-255. doi:10.1016/j.wasman.2016.04.003

74. Davidovits J. Geopolymers - Inorganic polymeric new materials. *Journal of Thermal Analysis*. 1991;37(8):1633-1656. doi:10.1007/BF01912193

75. Lancellotti I et al. Chemical stability of geopolymers containing municipal solid waste incinerator fly ash. *Waste Management*. 2010;30(4):673-679. doi:10.1016/J.WASMAN.2009.09.032

76. Zheng L, Wang W, Shi Y. The effects of alkaline dosage and Si/Al ratio on the immobilization of heavy metals in municipal solid waste incineration fly ash-based geopolymer. *Chemosphere*. 2010;79(6):665-671. doi:10.1016/J.CHEMOSPHERE.2010.02.018

77. Torres-Carrasco M, Puertas F. Waste glass in the geopolymer preparation. Mechanical and microstructural characterisation. *Journal of Cleaner Production*. 2015;90:397-408. doi: 10.1016/j.jclepro.2014.11.074

78. Novais R et al. Biomass fly ash geopolymer monoliths for effective methylene blue removal from wastewaters. *Journal of Cleaner Production*. 2018;171:783-794. doi:10.1016/j.jclepro.2017.10.078

79. He J et al. Synthesis and characterization of red mud and rice husk ash-based geopolymer composites. *Cem Concr Compos*. 2013;37(1):108-118. doi:10.1016/J.CEMCONCOMP.2012.11.010

80. Akbar A et al. Sugarcane bagasse ash-based engineered geopolymer mortar incorporating propylene fibers. *Journal of Building Engineering*. 2021;33. doi:10.1016/j.jobe.2020.101492

81. Rees C et al. In situ ATR-FTIR study of the early stages of fly ash geopolymer gel formation. *ACS Publications*. 2007;23(17):9076-9082. doi:10.1021/la701185g

82. Gladysz GM, Chawla KK. Characteristics and properties of porous materials. *Voids in Materials*. Published online 2021:189-229. doi:10.1016/B978-0-12-819282-5.00009-0

83. Ahmari S, Zhang L. The properties and durability of alkali-activated masonry units. *Handbook of Alkali-Activated Cements, Mortars and Concretes*. 2015:643-660. doi:10.1533/9781782422884.4.643

84. Saputra E et al. Geopolymer catalysts derived from palm oil mill ash for biodiesel production from Calophyllum inophyllum oil. *Applied Nanoscience*. 2022. doi:10.1007/s13204-021-02180-0

85. Rasaki SA et al. Geopolymer for use in heavy metals adsorption, and advanced oxidative processes: A critical review. *Journal of Cleaner Production*. 2018;12:145. doi:10.1016/j.jclepro.2018.12.145

86. Rahman MM, Law DW, Patnaikuni I. Optimizing the Mix Design of Clay Based Geopolymer Concrete. *Proceedings of International Structural Engineering and Construction.* 2016;3. doi:10.14455/ISEC.res.2016.128

87. Vasić MV et al. Alkali-activated geopolymerization of a low illitic raw clay and waste brick mixture. An alternative to traditional ceramics. *Appl Clay Sci*. 2022;218. doi:10.1016/J.CLAY.2022.106410

88. Tang Z et al. Mechanical performance of CFRP-confined sustainable geopolymeric recycled concrete under axial compression. *Eng Struct*. 2020;224:111246. doi:10.1016/J.ENGSTRUCT.2020.111246

89. Duan P, Yan C, Zhou W. Compressive strength and microstructure of fly ash based geopolymer blended with silica fume under thermal cycle. *Cem Concr Compos*. 2017;78:108-119. doi:10.1016/J.CEMCONCOMP.2017.01.009

90. Tome S et al. Characterization and Leachability Behaviour of Geopolymer Cement Synthesised from Municipal Solid Waste Incinerator Fly Ash and Volcanic Ash Blends. *Recycling*. 2018;3(4):50. doi:10.3390/RECYCLING3040050

91. Warwick C, Guerreiro A, Soares A. Sensing and analysis of soluble phosphates in environmental samples: A review. *Biosensors and Bioelectronics*. 2013;41:1-11. doi:10.1016/j.bios.2012.07.012

92. Rathour R et al. Treatment of various types of wastewaters using microbial fuel cell systems. *Microbial Electrochemical Technology*. 2019:665-692. doi:10.1016/B978-0-444-64052-9.00027-3

93. Soares M et al. Oil spill in South Atlantic (Brazil): Environmental and governmental disaster. *Mar Policy*. 2020;115:103879. doi:10.1016/J.MARPOL.2020.103879

94. Lu Y et al. Impacts of soil and water pollution on food safety and health risks in China. *Environment International*. 2015;77:5-15. doi:10.1016/j.envint.2014.12.010

95. Xiao L, Liu J, Jinwen G. Dynamic game in agriculture and industry cross-sectoral water pollution governance in developing countries. *Agricultural Water Management*. 2021;243. doi:10.1016/j.agwat.2020.106417

96. Englande AJ, Krenkel P, Shamas J. Wastewater Treatment & Water Reclamation. *Reference Module in Earth Systems and Environmental Sciences*. 2015. doi:10.1016/B978-0-12-409548-9.09508-7

97. Crini G, Lichtfouse E. Advantages and disadvantages of techniques used for wastewater treatment. *Environmental Chemistry Letters.* 2019;17:145-155. doi:10.1007/s10311-018-0785-9

98. Arsuaga JM et al. Temperature, pH and concentration effects on retention and transport of organic pollutants across thin-film composite nanofiltration membranes. *Desalination*. 2008;221:253-258. doi:10.1016/j.desal.2007.01.081

99. Hilma R et al. Determination of Total Phenolic, Flavonoid Content and free Radical Scavenging Activity of Etanol Extract Sawo Stem Bark. *Conference Proceedings CelSciTech-UMRI*. 2018;3.

100. Zahrani NA et al. Recent developments of gallic acid derivatives and their hybrids in medicinal chemistry: A review. *European Journal of Medicinal Chemistry*. 2020;204: 112609. doi:10.1016/j.ejmech.2020.112609

101. Bai J et al. Gallic acid: Pharmacological activities and molecular mechanisms involved in inflammation-related diseases. *Biomedicine and Pharmacotherapy*. 2021;133. doi:10.1016/j.biopha.2020.110985

102. Balasubramaniam SP et al. Fabrication of antioxidative food packaging films using cellulose nanofibers, kappa-Carrageenan, and gallic acid. *J Food Process Preserv*. 2021;45. doi:10.1111/jfpp.15480

103. Nam SH et al. Transglycosylation of gallic acid by using Leuconostoc glucansucrase and its characterization as a functional cosmetic agent. *AMB Express*. 2017;7. doi:10.1186/s13568-017-0523-x

104. Bassin JP et al. The impact of wastewater treatment plants on global climate change. *Water Conservation in the Era of Global Climate Change*. 2021;1:367-410. doi:10.1016/B978-0-12-820200-5.00001-4

105. Ding GKC. Wastewater Treatment, Reused and Recycling – A Potential Source of Water Supply. *Reference Module in Earth Systems and Environmental Sciences*. 2023. doi:10.1016/B978-0-323-90386-8.00062-0

106. Chai W et al. A review on conventional and novel materials towards heavy metal adsorption in wastewater treatment application. *Journal of Cleaner Production*. 2021;296. doi:10.1016/j.jclepro.2021.126589

107. Burakov A et al. Adsorption of heavy metals on conventional and nanostructured materials for wastewater treatment purposes: A review. *Ecotoxicology and Environmental Safety*. 2018;148:702-712. doi:10.1016/j.ecoenv.2017.11.034

108. Rathi B, Kumar PS. Application of adsorption process for effective removal of emerging contaminants from water and wastewater. *Environmental Pollution*. 2021;280. doi:10.1016/j.envpol.2021.116995

109. Liu X et al. Enhanced dyes adsorption from wastewater via Fe3O4 nanoparticles functionalized activated carbon. *Journal of Hazardous Materials*. 2019;373:397-407. doi:10.1016/j.jhazmat.2019.03.103

110. Bonilla-Petriciolet A, Mendoza-Castillo DI, Reynel-Ávila HE. Adsorption processes for water treatment and purification. *Adsorption Processes for Water Treatment and Purification*. 2017:1-256. doi:10.1007/978-3-319-58136-1/COVER

111. Crawford CB, Quinn B. The interactions of microplastics and chemical pollutants. *Microplastic Pollutants*. 2017:131-157. doi:10.1016/B978-0-12-809406-8.00006-2

112. Artioli Y. Adsorption. *Encyclopedia of Ecology, Five-Volume Set*. 2008:60-65. doi:10.1016/B978-008045405-4.00252-4

113. Do DD. Adsorption Analysis: Equilibria and Kinetics. 1998;2. doi:10.1142/P111

114. Tien C. Introduction to adsorption: Basics, analysis, and applications. 2018

115. Loganathan P et al. Defluoridation of drinking water using adsorption processes. *Journal of Hazardous Materials*. 2013;248:1-19. doi:10.1016/j.jhazmat.2012.12.043

116. Yagub M et al. Dye and its removal from aqueous solution by adsorption: a review. *Advances in Colloid and Interface Science*. 2014;209:172-184. doi:10.1016/j.cis.2014.04.002

117. Badawi MA et al. Adsorption of aluminum and lead from wastewater by chitosan-tannic acid modified biopolymers: Isotherms, kinetics, thermodynamics and process mechanism. *Int J Biol Macromol*. 2017;99:465-476. doi:10.1016/J.IJBIOMAC.2017.03.003

118. Albayati T, Alwan G, Mahdy O. High performance methyl orange capture on magnetic nanoporous MCM-41 prepared by incipient wetness impregnation method. *Korean Journal of Chemical Engineering*. 2017;34(1):259-265. doi:10.1007/s11814-016-0231-2

119. Nasiri Azad F et al. Preparation and characterization of MWCNTs functionalized by N-(3-nitrobenzylidene)-N′-trimethoxysilylpropyl-ethane-1,2-diamine for the removal of aluminum(III) ions via complexation with eriochrome cyanine R: spectrophotometric detection and optimization. *RSC Adv*. 2015;5(75):61060-61069. doi:10.1039/C5RA08746E

120. Bhatt AS et al. Adsorption of an anionic dye from aqueous medium by organoclays: equilibrium modeling, kinetic and thermodynamic exploration. *RSC Adv*. 2012;2(23):8663-8671. doi:10.1039/C2RA20347B

121. Sturm P et al. Synthesizing one-part geopolymers from rice husk ash. *Construction and Building Materials*. 2016;124:961-966. doi:10.1016/j.conbuildmat.2016.08.017

122. Prachasaree W et al. Development of equivalent stress block parameters for fly-ash-based geopolymer concrete. *Arabian Journal for Science and Engineering*. 2014;39(12):8549-8558. doi:10.1007/s13369-014-1447-2

123. Wang C et al. Quantifying gel properties of industrial waste-based geopolymers and their application in Pb2+ and Cu2+ removal. *Journal of Cleaner Production*. 2021;315. doi:10.1016/j.jclepro.2021.128203

124. Chen S et al. Efficient removal of radioactive iodide anions from simulated wastewater by HDTMA-geopolymer. *Progress in Nuclear Energy*. 2019;117. doi:10.1016/j.pnucene.2019.103112

125. Mužek MN, Svilović S, Zelić J. Fly ash-based geopolymeric adsorbent for copper ion removal from wastewater. *Desalination Water Treat*. 2014;52(13-15):2519-2526. doi:10.1080/19443994.2013.792015

126. Javadian H, Ghorbani F, Tayebi H allah, Asl SMH. Study of the adsorption of Cd (II) from aqueous solution using zeolite-based geopolymer, synthesized from coal fly ash; kinetic, isotherm and thermodynamic studies. *Arabian Journal of Chemistry*. 2015;8(6):837-849. doi:10.1016/J.ARABJC.2013.02.018

127. Lee NK, Khalid HR, Lee HK. Adsorption characteristics of cesium onto mesoporous geopolymers containing nano-crystalline zeolites. *Microporous and Mesoporous Materials*. 2017;242:238-244. doi:10.1016/J.MICROMESO.2017.01.030

128. Sarkar C, Basu JK, Samanta AN. Removal of Ni2+ ion from waste water by Geopolymeric Adsorbent derived from LD Slag. *Journal of Water Process Engineering*. 2017;17:237-244. doi:10.1016/J.JWPE.2017.04.012

129. Kara I et al. Study on the performance of metakaolin based geopolymer for Mn(II) and Co(II) removal. *Appl Clay Sci*. 2018;161:184-193. doi:10.1016/J.CLAY.2018.04.027

130. Novais RM et al. Synthesis of porous biomass fly ash-based geopolymer spheres for efficient removal of methylene blue from wastewaters. *J Clean Prod*. 2019;207:350-362. doi:10.1016/J.JCLEPRO.2018.09.265

131. Srinivasa AS, Swaminathan K, Yaragal SC. Microstructural and optimization studies on novel one-part geopolymer pastes by Box-Behnken response surface design method. *Case Studies in Construction Materials*. 2023;18. doi:10.1016/j.cscm.2023.e01946

132. Rao JS, Kumar B. *3D Blade Root Shape Optimization*. 2012

133. Kara İ, Yilmazer D, Akar ST. Metakaolin based geopolymer as an effective adsorbent for adsorption of zinc(II) and nickel(II) ions from aqueous solutions. *Appl Clay Sci*. 2017;139:54-63. doi:10.1016/j.clay.2017.01.008

134. Jin H et al. Rapid removal of methylene blue and nickel ions and adsorption/desorption mechanism based on geopolymer adsorbent. *Colloids and Interface Science Communications*. 2021;45. doi:10.1016/j.colcom.2021.100551

135. Onutai S et al. Porous fly ash-based geopolymer composite fiber as an adsorbent for removal of heavy metal ions from wastewater. *Materials Letters*. 2019;236:30-33. doi:10.1016/j.matlet.2018.10.035

136. Duan P et al. Development of fly ash and iron ore tailing based porous geopolymer for removal of Cu(II) from wastewater. *Ceram Int*. 2016;42(12):13507-13518. doi:10.1016/j.ceramint.2016.05.143

137. Ariffin N et al. Effect of aluminium powder on kaolin-based geopolymer characteristic and removal of Cu2+. *Materials*. 2021;14(4):1-19. doi:10.3390/ma14040814

138. Aouan B et al. Application of central composite design for optimisation of the development of metakaolin based geopolymer as adsorbent for water treatment. *Int J Environ Anal Chem*. 2022. doi:10.1080/03067319.2022.2070010

139. Complejo Medioambiental de Cerceda | Sogama. Accessed July 28, 2022. https://www.sogama.gal/el-complejo-medioambiental-de-cerceda

140. Li L, Wang S, Zhu Z. Geopolymeric adsorbents from fly ash for dye removal from aqueous solution. *J Colloid Interface Sci*. 2006;300(1):52-59. doi:10.1016/J.JCIS.2006.03.062

141. Al-Zboon K, Al-Harahsheh MS, Hani FB. Fly ash-based geopolymer for Pb removal from aqueous solution. *J Hazard Mater*. 2011;188(1-3):414-421. doi:10.1016/J.JHAZMAT.2011.01.133

142. Siyal AA et al. Fly ash based geopolymer for the adsorption of anionic surfactant from aqueous solution. *J Clean Prod*. 2019;229:232-243. doi:10.1016/J.JCLEPRO.2019.04.384

143. Chen K, Lin WT, Liu W. Effect of NaOH concentration on properties and microstructure of a novel reactive ultra-fine fly ash geopolymer. *Advanced Powder Technology*. 2021;32(8):2929-2939. doi:10.1016/J.APT.2021.06.008

144. Feng X et al. Green Synthesis of the Metakaolin/slag Based Geopolymer for the Effective Removal of Methylene Blue and Pb (II). *Silicon*. 2022;14: 6965–6979 doi:10.1007/s12633-021-01439-z

145. Król M, Minkiewicz J, Mozgawa W. IR spectroscopy studies of zeolites in geopolymeric materials derived from kaolinite. *J Mol Struct*. 2016;1126:200-206. doi:10.1016/J.MOLSTRUC.2016.02.027

146. Panda L, et al. Thorough understanding of the kinetics and mechanism of heavy metal adsorption onto a pyrophyllite mine waste based geopolymer. *J Mol Liq*. 2018;263:428-441. doi:10.1016/J.MOLLIQ.2018.05.016

147. Azhari E et al. Synthesis, Characterization, and Application of Geopolymer/TiO2 Nanoparticles Composite for Efficient Removal of Cu(II) and Cd(II) Ions from Aqueous Media. 2022;12(11):1445. doi:10.3390/MIN12111445

148. Riahi S et al. The effect of mixing molar ratios and sand particles on microstructure and mechanical properties of metakaolin-based geopolymers. *Mater Chem Phys*. 2020;240. doi:10.1016/j.matchemphys.2019.122223

149. Tian Q, Sasaki K. Application of fly ash-based geopolymer for removal of cesium, strontium and arsenate from aqueous solutions: kinetic, equilibrium and mechanism analysis. *Water Science and Technology*. 2019;79(11):2116-2125. doi:10.2166/WST.2019.209

150. Purbasari A, Ariyanti D, Sumardiono S. Preparation and application of fly ash-based geopolymer for heavy metal removal. *AIP Conference Proceedings*. 2020;2197:050006. doi:10.1063/1.5140918

151. Zhu C, Xu Q. Amorphous Materials for Enhanced Localized Surface Plasmon Resonances. *Chem Asian J*. 2018;13(7):730-739. doi:10.1002/asia.201701722

152. Wan H et al. Slag-based geopolymer microspheres as a support for CO2 methanation. *Fuel*. 2022;319. doi:10.1016/j.fuel.2022.123627

153. Shao N et al. Fabrication of hollow microspheres filled fly ash based foam geopolymers with ultra-low thermal conductivity and relative high strength. *Constr Build Mater*. 2018;185:567-573. doi:10.1016/j.conbuildmat.2018.07.077

154. Shao NN et al. Fabrication of hollow microspheres filled fly ash geopolymer composites with excellent strength and low density. *Mater Lett*. 2015;161:451-454. doi:10.1016/j.matlet.2015.09.016

155. Jahani D et al. Polyvinyl alcohol/calcium carbonate nanocomposites as efficient and cost-effective cationic dye adsorbents. *Polymers (Basel)*. 2020;12(10). doi:10.3390/POLYM12102179

156. Ahmad K et al. Removal of Heavy Metals (Zn, Cr, Pb, Cd, Cu and Fe) in Aqueous Media by Calcium Carbonate as an Adsorbent. *International Journal of Chemical and Biochemical Sciences*. 2012;2:48-53.

157. Zhao DH, Gao HW. Turning calcium carbonate into a cost-effective wastewater-sorbing material by occluding waste dye. *Environmental Science and Pollution Research*. 2010;17(1):97-105. doi:10.1007/s11356-009-0111-y

158. Fernández-Jiménez A, Palomo A. Composition and microstructure of alkali activated fly ash binder: Effect of the activator. *Cem Concr Res*. 2005;35(10):1984-1992. doi:10.1016/J.CEMCONRES.2005.03.003

159. Khatib K, Kerroumi H, El Azhari M. Synthesis, characterization and optimization of new adsorbent materials based on industrial discharges for the decontamination of liquid effluents. *Mater Today Proc*. 2020;22:120-125. doi:10.1016/J.MATPR.2019.08.120

160. Siyal AAet al. Adsorption Kinetics, Isotherms, and Thermodynamics of Removal of Anionic Surfactant from Aqueous Solution Using Fly Ash. *Water, Air, & Soil Pollution*. 2020;231:509. doi:10.1007/s11270-020-04879-2

161. Kipton H, Powell J, Taylor MC. Interactions of iron(II) and iron(III) with gallic acid and its homologues: a potentiometric and spectrophotometric study. *Aust J Chem*. 1982;35(4):739-756. doi:10.1071/CH9820739

162. Celestino GG et al. Adsorption of gallic acid on nanoclay modified with poly(diallyldimethylammonium chloride). *Environmental Science and Pollution Research*. 2019;26(28):28444-28454. doi:10.1007/S11356-018-3505-X/TABLES/4

163. Darmayanti L et al. Structural alteration within fly ash-based geopolymers governing the adsorption of Cu2+ from aqueous environment: Effect of alkali activation. *J Hazard Mater*. 2019;377:305-314. doi:10.1016/j.jhazmat.2019.05.086

164. Zhang Y, Liu L. Fly ash-based geopolymer as a novel photocatalyst for degradation of dye from wastewater. *Particuology*. 2013;11(3):353-358. doi:10.1016/j.partic.2012.10.007

165. da Costa Rocha AC et al. Economical and Technological Aspects of Copper Removal from Water Using a Geopolymer and Natural Zeolite. *Water Air Soil Pollut*. 2020;231(7). doi:10.1007/s11270-020-04722-8

166. Purbasari A et al. Adsorption Kinetics and Isotherms of Cu(Ii) and Fe(Ii) Ions from Aqueous Solutions by Fly Ash-Based Geopolymer. *Chemistry and Chemical Technology*. 2022;16(2):169-176. doi:10.23939/chcht16.02.169

167. Liu Y et al. A comparative study on fly ash, geopolymer and faujasite block for Pb removal from aqueous solution. *Fuel*. 2016;185:181-189. doi:10.1016/j.fuel.2016.07.116

168. Hasani N et al. Theoretical, Equilibrium, Kinetics and Thermodynamic Investigations of Methylene Blue Adsorption onto Lignite Coal. *Molecules*. 2022;27(6):1856. doi:10.3390/MOLECULES27061856

169. Duan P et al. Development of fly ash and iron ore tailing based porous geopolymer for removal of Cu(II) from wastewater. *Ceram Int*. 2016;42(12):13507-13518. doi:10.1016/j.ceramint.2016.05.143

170. Tian Q, Sasaki K. Application of fly ash-based geopolymer for removal of cesium, strontium and arsenate from aqueous solutions: Kinetic, equilibrium and mechanism analysis. *Water Science and Technology*. 2019;79(11):2116-2125. doi:10.2166/wst.2019.209

171. Qiu J et al. Fly ash-based geopolymer as a potential adsorbent for Cr(VI) removal. *Desalination Water Treat*. 2017;70:201-209. doi:10.5004/dwt.2017.20493

172. Purbasari A, Ariyanti D, Fitriani E. Adsorption of anionic and cationic dyes from aqueous solutions on fly ash-based porous geopolymer. *Global NEST Journal*. 2023. doi:10.30955/gnj.004363

173. Ho YS, Porter JF, Mckay G. Equilibrium Isotherm Studies for the Sorption of Divalent Metal Ions onto Peat: Copper, Nickel and Lead Single Component Systems. 2002;141:1-33. doi:10.1023/A:1021304828010